Am J Cancer Res 2021;11(9):4141-4174
www.ajcr.us /ISSN:2156-6976/ajcr0135005

Original Article

Bio-nanoparticle based therapeutic vaccine induces immunogenic response against triple negative breast cancer

Xuewei Bai[1,2*], Yanmei Zhou[1,3*], Qiushi Lin[4], Chiung-Kuei Huang[1], Songhua Zhang[1], Rolf I Carlson[1], Hossein Ghanbari[5], Bei Sun[2], Jack R Wands[1], Xiaoqun Dong[1]

[1]Liver Research Center, Rhode Island Hospital, Department of Medicine, The Warren Alpert Medical School, Brown University, Providence, RI 02903, USA; [2]Department of Pancreatic and Biliary Surgery, Key Laboratory of Hepatosplenic Surgery, Ministry of Education, The First Affiliated Hospital of Harbin Medical University, Harbin 150081, Heilongjiang Province, P. R. China; [3]Department of Anesthesiology, The First Affiliated Hospital of Harbin Medical University, Harbin 150081, Heilongjiang Province, P. R. China; [4]Yurogen Biosystems LLC, 1 Innovation Dr Suite 115, Worcester, MA 01605, USA; [5]Athanor Biosciences, Inc. 1448 S. Rolling Rd., Suite 021, Halethorpe, MD 21227, USA. [*]Equal contributors.

Received May 7, 2021; Accepted June 18, 2021; Epub September 15, 2021; Published September 30, 2021

Abstract: Triple negative breast cancer (TNBC) is more aggressive and has a poorer prognosis than other sub-types of breast tumors. This study elucidates how aspartate beta-hydroxylase (ASPH) network promotes drug resistance, and immunotherapy targeting ASPH may improve the efficacy of Doxorubicin (DOX) therapy. An orthotopic model of breast cancer generated by 4T1 cells in immunocompetent mice was used to explore efficacy of immunotherapy in combination with DOX chemotherapy. We evaluated mRNA and protein expression in cultured tumor cells and tissue, as well as assessed cell proliferation, apoptosis, soluble factors/cytokine production, immune cell population diversity and function. We observed that ASPH expression enables TNBC cells to exhibit primary resistance to DOX induced single-/double-strand breaks (SSB/DSB) and enhanced proliferation and survival. Specific bio-nanoparticle based therapeutic vaccine (BNP-TV) promoted ASPH uptake by and maturation of DCs. This BNP-TV combined with DOX induces immunogenic cell death (ICD) in orthotopic xenograft tumors and significantly suppressed primary mammary tumor growth and distant multi-organ metastases. Immunogenic cell death induced by BNP-TV targeting ASPH combined with DOX provides opportunities to treat a highly resistant and metastatic form of breast cancer.

Keywords: Aspartate β-hydroxylase, metastasis, λ-phage, doxorubicin, immunogenic cell death

Introduction

Breast cancer is the most common malignancy and the second leading cause of mortality in women worldwide. In 2018, 2,088,849 new cases were diagnosed globally, accounting for 25.4% of a panoply of cancers (except non-melanoma skin cancer) in women. Despite advancement in surgery, chemotherapy, targeted therapy and radiotherapy, 40,920 patients died of advanced breast cancer in 2018 [1]. Therefore, it is paramount to explore effective therapy to treat aggressive and refractory disease. Recent emergence of immunotherapy has demonstrated potency of the immune system as a therapeutic modality for a number of human tumors.

As a classical chemotherapeutic agent for breast cancer treatment, DOX inhibits the progression of topoisomerase II (which relaxes supercoils in DNA for transcription) and thus impairs macromolecular biosynthesis. The DOX stabilizes the topoisomerase II complex after it has broken the DNA chain for replication, preventing the DNA double helix from being resealed. Intercalation of DOX induces histone eviction from transcriptionally active chromatin, leading to deregulated DNA damage response, epigenome and transcriptome in cancer cells [2].

As a form of cell death (apoptosis), ICD is caused by cytostatic agents (e.g., anthracyclines [3, 4], mitoxantrone, oxaliplatin and bort-

ezomib), radiotherapy or photodynamic therapy [5]. The ICD induces an effective antitumor immune response through activation of dendritic cells (DCs) and consequent activation of specific T cell response. The dying cells release damage associated molecular patterns (DAMPs) to recruit and activate DCs [6]. The activated DCs recruit more immune cells and present antigens to naive T cells, which induce T cells to differentiate, mature and secrete interferon gamma (IFNγ) to destroy tumor cells.

Bacteriophage display presents foreign amino acids (peptides) in immunologically assessable form to the immune system [7]. Bacteriophage lambda (λ) stably displays fusion proteins on its capsid protein, containing copious copies of antigenic peptides [8]. The high-density display of foreign proteins on bacteriophage λ efficiently demonstrate low-affinity protein-protein interactions [8].

Notably, ASPH is highly expressed in majority of breast cancer, especially in triple negative and HER2 amplification subtypes [9]. Importantly, exogenous overexpression of ASPH portend more aggressive phenotypes and reduces overall and disease-free survival of breast cancer patients [9]. Mechanistically, ASPH promotes tumor cell proliferation, migration, invasion, and metastasis [10-12]. Here, we hypothesized that an ASPH-based vaccine, in combination with doxorubicin, will produce synergistic antitumor immune responses.

Materials and methods

Cell lines

Human (MDA-MB-231 and SK-BR-3) or murine (4T1) breast cancer cell lines were purchased from American Type Culture Collection. Cells were cultured at 37°C in a humidified atmosphere containing 5% CO_2 in corresponding medium supplemented with 2 mM glutamine, 10% FBS and antibiotics (penicillin and streptomycin). Stable MDA-MB-231 cell lines (**Figure 1A**) overexpressing ASPH or empty vector were established using the lentiviral system (GeneCopoeia, #EX-Z8758-Lv105). ASPH knock-down ("KD") SK-BR-3 cell lines (**Figure 1B**) were established using plasmids pLKO.1-shRNA-luciferase (shLuc) and pLKO.1-shRNA-ASPH from Dharmacon (Lafayette, CO).

Antibodies and reagents

The rabbit polyclonal antibody of ASPH and a small molecular inhibitor (1182) of ASPH enzymatic activity were developed as previously described [13]. Doxorubicin was purchased from Pfizer Inc. The α-ketoglutarate (α-KG), Bouin's fixative solution, thiazolyl blue tetrazolium blue (MTT) and methylene blue were purchased from Sigma-Aldrich (St. Louis, MO). Antibodies used for Western blot assays are listed in **Table 1**. The ASPH-based λ phage vaccine (BNP-TV) has been developed and synthesized by Sensei Therapeutics as described previously [14]. In brief, a bacteriophage λ system was designed to display ASPH fused at C-terminus of capsid protein gpD. Due to limitations on the size of DNA that can be incorporated into viable λ phage, ASPH sequence was divided to 3 segmented allowing for proper display of ASPH peptides on λ head. This study focuses on both N- and C-terminal regions of ASPH protein, designated as ASPH constructs λ1 and λ3, respectively. Using specific oligo primers, 3 segments were amplified from the ASPH gene. The oligo sequence of primer was modified to produce restriction sites for Nhe I and Bssh II enzymes at the end of each segment. After restriction enzyme digestion, this segment was inserted at NheI-BsshII site of the 3' end of a DNA segment encoding GpD under the control of lac promoter. These constructs were created in donor plasmid pVCDcDL1A, with *loxPwt* and *loxP511* sequences. *Cre*-expressing *E. coli* was transformed with recombinant plasmids and subsequently infected with recipient λ phage DL1 (λ-DL1) that carried a stuffer DNA segment flanked by *loxPwt* and *loxP511* sites. Recombination occurred *in vivo* at the *lox* sites, and then *Ampr* cointegrates were formed, which spontaneously lysed *E. coli* and released products in culture media. These cointegrates produced recombinant phages that display ASPH peptides fused at C-terminus of GpD. Recombination with unmodified pVCDcDL3 alone yielded control phage particles without display of ASPH peptides.

Real-time quantitative PCR (RT-qPCR)

Cells were lysed with 1 ml TRIzol (Thermo Fisher Scientific, #15596026) at room temperature for 30 min. Total RNA was extracted from

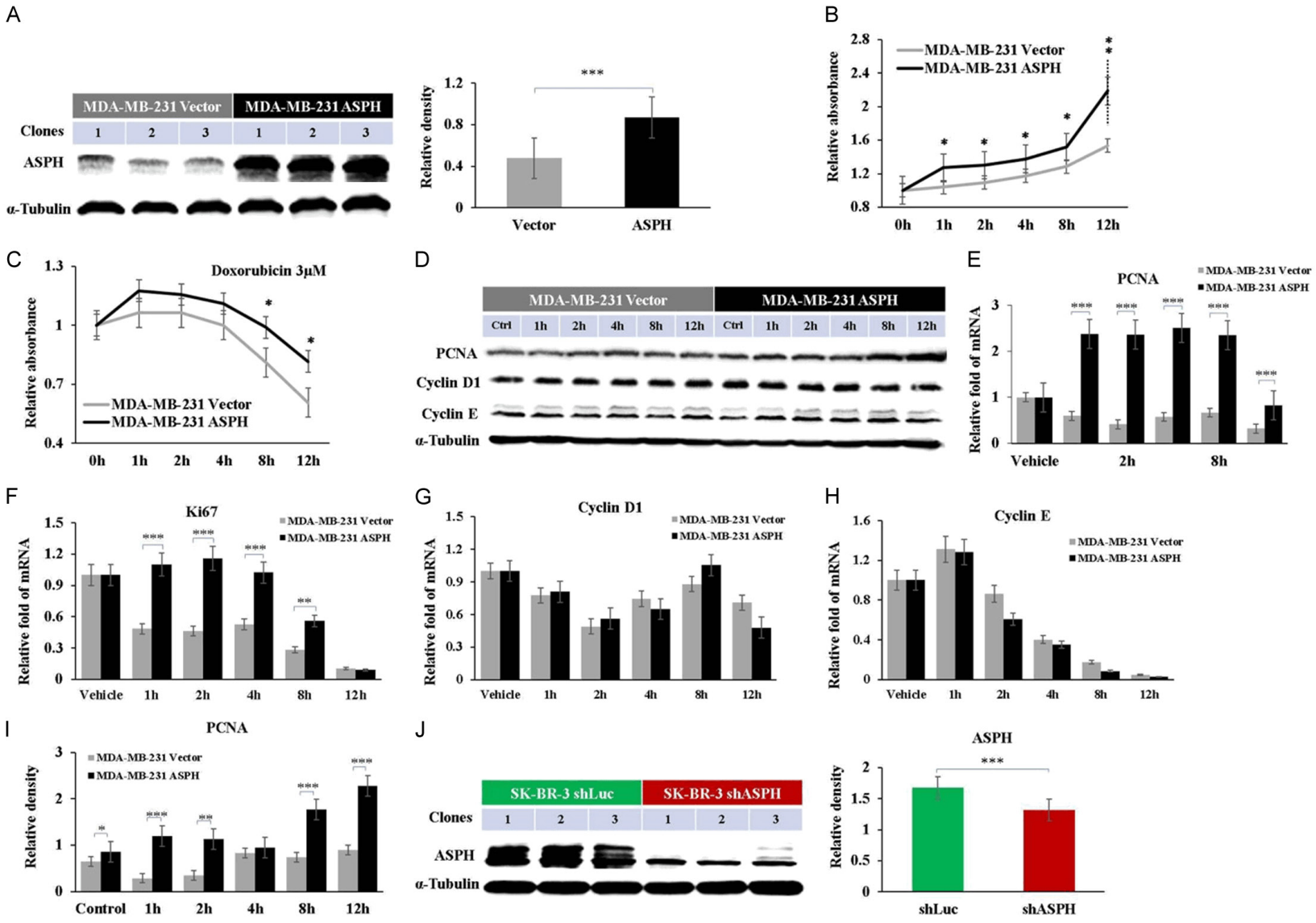
A
MDA-MB-231 Vector
MDA-MB-231 ASPH
Clones
1
2
3
1
2
3
ASPH
α-Tubulin
Relative density
***
1.2
0.8
0.4
0
Vector
ASPH
B
MDA-MB-231 Vector
MDA-MB-231 ASPH
Relative absorbance
2.8
2.4
2
1.6
1.2
0.8
0h
1h
2h
4h
8h
12h
C
Doxorubicin 3μM
Relative absorbance
1.3
1
0.7
0.4
MDA-MB-231 Vector
MDA-MB-231 ASPH
0h
1h
2h
4h
8h
12h
D
MDA-MB-231 Vector
MDA-MB-231 ASPH
Ctrl
1h
2h
4h
8h
12h
PCNA
Cyclin D1
Cyclin E
α-Tubulin
E
PCNA
MDA-MB-231 Vector
MDA-MB-231 ASPH
Relative fold of mRNA
3
2
1
0
Vehicle
2h
8h
F
Ki67
MDA-MB-231 Vector
MDA-MB-231 ASPH
Relative fold of mRNA
1.5
1.2
0.9
0.6
0.3
0
Vehicle
1h
2h
4h
8h
12h
G
Cyclin D1
MDA-MB-231 Vector
MDA-MB-231 ASPH
Relative fold of mRNA
1.5
1.2
0.9
0.6
0.3
0
Vehicle
1h
2h
4h
8h
12h
H
Cyclin E
MDA-MB-231 Vector
MDA-MB-231 ASPH
Relative fold of mRNA
1.6
1.2
0.8
0.4
0
Vehicle
1h
2h
4h
8h
12h
I
PCNA
MDA-MB-231 Vector
MDA-MB-231 ASPH
Relative density
3
2
1
0
Control
1h
2h
4h
8h
12h
J
SK-BR-3 shLuc
SK-BR-3 shASPH
Clones
1
2
3
1
2
3
ASPH
α-Tubulin
ASPH
***
Relative density
2
1.5
1
0.5
0
shLuc
shASPH

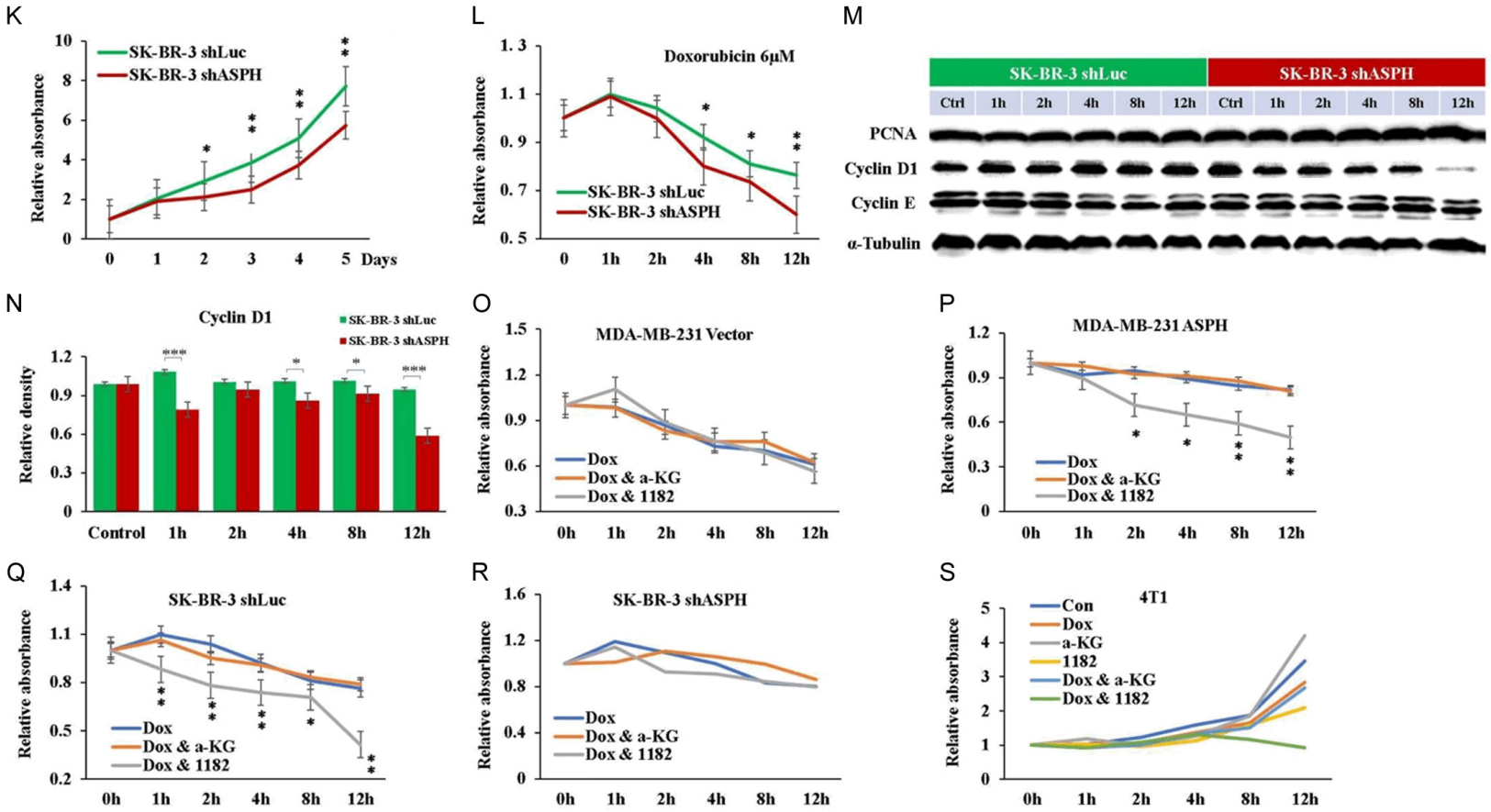

Figure 1. ASPH mediates resistance to Doxorubicin by enhancing proliferation in breast cancer cells. (A) Stable MDA-MB-231 cell lines overexpressing ASPH vs. empty vector. (B, C) Growth curves of MDA-MB-231 cell lines in response to DOX as measured by MTT assays. (D) Dynamic changes in biomarkers for cell cycle progression (proliferation) in response to DOX in MDA-MB-231 cell lines. (E-I) Quantification of elements expression at mRNA and protein levels by qPCR or Western blot. (I) Quantification (normalized to α-tubulin) of PCNA protein expression in (D), which is dynamically changed over time. (J) Knocking-down ASPH in SK-BR-3 cell lines. (K, L) Growth curves of SK-BR-3 cell lines in response to DOX as measured by MTT assays. (M) Dynamic changes in biomarkers for cell cycle progression (proliferation) in response to DOX in SK-BR-3 cell lines. (N) Quantification of elements expression in (M). (O-S) Growth curves of breast cancer cell lines in response to DOX, α-Ketoglutarate, SMI alone or in combination as measured by MTT assays. $^{*}P<0.05$; $^{**}P<0.01$; $^{***}P<0.001$ compared to corresponding control. Data were expressed as mean ± SD calculated from each experiment performed in triplicate under each condition.

Table 1. Reagents used in this study

Reagent	Company	Cat log#
ASPH	Homemade	
r-H_2AX	Cell Signaling Technology	9718
GADD45a	Cell Signaling Technology	4632
Cleaved PARP	Cell Signaling Technology	5625 and 94885
PCNA	Abcam	ab92552
Cyclin D1	Cell Signaling Technology	2978
Cyclin E	Thermo Fisher Scientific	MA5-14336
Bcl-2	Cell Signaling Technology	3498
Bcl-xL	Cell Signaling Technology	2764
Cleaved caspase-3 (Asp175)	Cell Signaling Technology	9661
p-Mre11 (Ser676)	Cell Signaling Technology	4859
Mre11	Cell Signaling Technology	4895
p-Rad50	Cell Signaling Technology	14223
Rad50	Cell Signaling Technology	3427
p-NBS1 (Ser343)	Cell Signaling Technology	3001
NBS1	Cell Signaling Technology	3002
p-ATM (Ser1981)	Cell Signaling Technology	5883
ATM	Cell Signaling Technology	2873
p-AMPK (Thr172)	Cell Signaling Technology	2531
HIPK2	Cell Signaling Technology	5091
p-P53 (Ser46)	Cell Signaling Technology	2521s
P53	Cell Signaling Technology	9282
eIF2A	Thermo Fisher Scientific	44-728G
Calreticulin	Thermo Fisher Scientific	PA3-900
HMGB1	Thermo Fisher Scientific	PA5-27378
LRP1	Thermo Fisher Scientific	No. 37-7600
TLR4	Thermo Fisher Scientific	No. 710185

Table 2. Primers for RT-qPCR assays

Gene Name	species	Label	Primer Sequence
PCNA	Human	h-PCNA-F	CCTGCTGGGATATTAGCTCCA
PCNA	Human	h-PCNA-R	CAGCGGTAGGTGTCGAAGC
MKI67	Human	h-MKI67-F	GCCTGCTCGACCCTACAGA
MKI67	Human	h-MKI67-R	GCTTGTCAACTGCGGTTGC
cyclin D1	Human	h-CCND1-Q-F (Ex1-2)	CCTCGGTGTCCTACTTCAAATG
cyclin D1	Human	h-CCND1-Q-R (Ex1-2)	CACTTCTGTTCCTCGCAGAC
cyclin E	Human	h-CCNE1-F	GCCAGCCTTGGGACAATAATG
cyclin E	Human	h-CCNE1-R	CTTGCACGTTGAGTTTGGGT
HRK	Human	h-HRK-F	GGCAGGCGGAACTTGTAGGAAC
HRK	Human	h-HRK-R	TCCAGGCGCTGTCTTTACTCTCC
BIM	Human	h-Bim-F	TAAGTTCTGAGTGTGACCGAGA
BIM	Human	h-Bim-R	GCTCTGTCTGTAGGGAGGTAGG

lysed cells according to the manufacture's instruction. 1 μg of total RNA was used to perform reverse transcription with iScript™ cDNA Synthesis Kit (Bio-Rad, #17-08891). The primers (**Table 2**) were used to amplify the genes of interest. The RT-qPCR reactions were performed with SYBR green master mix reagent. Relative changes in gene expression were analyzed with $2^{-\Delta\Delta CT}$ protocol.

Western blotting

Tumor tissues and cells were lysed with radioimmunoprecipitation buffer (Thermo Fisher Scientific, #89901) and quantified with Pierce BCA Protein Assay Kit (Thermo Fisher Scientific, #23-225). Protein samples (50 μg) were mixed with loading buffers, boiled at 100°C for 5 min, and immediately cooled down on ice for 5 min. To detect ATM/p-ATM (Ser1981), 6% SDS-PAGE gel was adopted to resolve samples, whereas 8% gels for Rad50 and HIPK2, 10% gels for ASPH, Mre11/p-Mre11 (Ser676), NBS1/p-NBS1 (Ser343), cleaved PARP, p-AMPK (Thr172) and calreticulin, 12% gel for Cyclin E, Cyclin D1, p-P53 (Ser46), PCNA, Bcl-2, Bcl-xl, GADD45α and p-eIF2A (Ser-52); 15% gel for γ-H_2AX, cleaved caspase-3 and HMGB1. The primary antibodies were diluted at a ratio of 1:1000 to cover the PVDF membranes and incubated overnight at 4°C. The secondary antibodies were anti-mouse-conjugated with HRP (Santa Cruz Biotechnology, 1:3000) and anti-rabbit-conjugated with HRP (Santa Cruz Biotechnology, 1:5000). The α-tubulin served as internal control. Protein expression was developed by enhanced chemiluminescence ECL Western blotting system

(Thermo Fisher Scientific, #34096). The relative density of bands was analyzed by NIH ImageJ software.

MTT

Breast cancer cells were seeded into 96-well plates (3000 cells/well), allowed to attach for 24 h, and treated with α-KG (25 μM), doxorubicin (3 μM for MDA-MB-231; 6 μM for SK-BR-3 and 4T1), or 1182 (1 μM). Culture medium was changed daily for 5 days. The MTT solution was prepared with sterile PBS (5 mg/ml). The MTT solution was diluted (1:10) into culture medium. Culture media with MTT solution were added to 96-well plates and incubated for 1 h. The solution containing dissolved MTT crystal with DMSO was measured at OD570 nanometer. The relative cell growth rate was calculated using the values at OD570. The relative absorbance of each well = absolute absorbance/control. All experiments were performed in triplicate wells for each condition and repeated in triplicate.

TUNEL

The TUNEL Colorimetric IHC Detection Kit (Thermo Fisher Scientific, #C10625) was used. Deparaffinize tissue section in 1× PBS was incubated with proteinase K for 10-20 min at room temperature. The slides were washed in 1× PBS for 3 times and incubated with TdT reaction buffer for 10 min at 37°C. Then, 50 μl TdT reaction mixture was added to slides and incubated for 60 min at 37°C. The TdT reaction was quenched with endogenous peroxidase enzymes. The slides were washed with TUNEL wash solution and incubated with TUNEL reaction mixture for 30 minutes at 37°C. The slides were washed and streptavidin-peroxidase conjugate were added to completely cover the samples at room temperature for 30 min. The slides were washed and 100 μl 1× DAB reaction mixture was added to cover the samples for 2 min at room temperature. Hematoxylin (H-3404, Vector Laboratories Inc.) was used to counterstain. Images were analyzed by NIH ImageJ software. All experiments were performed in triplicate wells for each condition and repeated in triplicate.

Enzyme-linked immunosorbent assay (ELISA)

Whole blood was collected from the heart after euthanasia and centrifuged at 3000 rpm for 20 min. Serum samples were collected and frozen at -20°C. The IFNγ ELISA Kit (Thermo Fisher Scientific, #KMC4021) and HMGB1 ELISA Kit (Aviva Systems Biology, #OKCD-04072; #OKCD04074) were applied to serum or supernatant of cell culture after serial dilutions (1:4). Then, 100 μL of standard, control, or samples were added to each well and incubated for 2 h at room temperature. The solution was thoroughly aspirated and wells washed for 4 times with 1× PBS buffer. Immediately, 100 μL mouse IFN-γ biotin conjugate solution was added into each well and incubated for 1 h at room temperature. 100 μL 1× streptavidin-HRP solution was added into each well and incubated for 30 min at room temperature. Each well was washed and 100 μL stabilized chromogen was added to develop. The absorbance was read at 450 nm after adding stop solution. The concentrations of samples were calculated according to the standard curve. All experiments were performed in triplicate wells for each condition and repeated in triplicate.

Immunohistochemistry (IHC) & immunofluorescence (IF)

Tumor cells were seeded on coverslip embedded with glycine, fixed in 4% formaldehyde and stained. Tumor tissues were fixed in 4% formaldehyde, embedded in paraffin, and prepared into 4-μm-thick slices. The antigen was retrieved and endogenous peroxidase activity was quenched through a 30-minute treatment in methanol with 3% hydrogen peroxide. Nonspecific antigen was blocked for 1 h. The slices were incubated with primary antibodies overnight at 4°C. After a rinse, HRP (Vector Laboratories, #PK4001 and #PK-6102) or fluorescent second antibody (Thermo Fisher Scientific, #RMG101 and #A24538) was added into the slices and incubated for 1 h. For IF, the slices were mounted with DAPI (Vector Laboratories, #H-1800) and observed under a fluorescence microscope. For IHC, the slices were incubated with peroxidase-labeled for 30 minutes, secondary antibody developed with DAB Kit (SK-4100, Vector Laboratories) and counterstained with hematoxylin. For quantitation, 5 microscopic fields were randomly selected at 400× magnification. Images were analyzed by ImageJ software (National Institutes of Health, Bethesda, Maryland, USA, https://imagej.nih.gov/ij/).

Orthotopic murine models of breast cancer

This study has been approved by the Institutional Animal Care and Use Committee at Rhode Island Hospital. Totally 40 female, 6-8-week-old BALB/c mice (Charles River Laboratories, Wilmington, MA) were randomly divided into four groups (n=10/group): control, DOX, Vaccine and DOX+Vaccine (combination). 4T1 cells (5×10^4/50 μl PBS) were subcutaneously inoculated into the right forth mammary fat pad of mice. From day 7, mice in Vaccine and combination groups simultaneously received λ phage particles (1×10^{10} pfu) suspended in 100 μL of PBS into the base of tails, once a week for 4 weeks. From day 15 after inoculation, doxorubicin (1 mg/kg) or PBS (control) was intraperitoneally (i.p.) administered in DOX and DOX+Vaccine groups three times a week for 4 weeks. Body weight and tumor volume ($\frac{length \times width \times width}{2}$) were measured twice a week. At 7 weeks after inoculating 4T1 cells, mice were euthanized; whole blood, primary tumors, lungs, spleen and other tissue samples were harvested. The number and size of macro-metastatic lesions in the lungs (immersed in Bouin's fixative solution) were counted and measured. Serum samples were collected following centrifugation and stored at -80°C. Tumors were excised and fixed with 10% formalin for IHC analysis.

In vitro cytotoxicity

Spleen tissues of BALB/c mice from control and Vaccine groups were dispersed into cell suspension. Lysis solution buffer was applied to delete erythrocytes. The isolated spleen cells were co-cultured with 4T1 cells for 5 h. Lymphocytic cytotoxicity was measured with a detection kit (Sigma-Aldrich, #4744926001) as described previously [15].

Flow cytometry

Isolated splenocytes (1×10^6 cells/mL) from the 4T1 tumor bearing mice were re-stimulated with 0.4 μg/ml rASPH ± 2×10^8 pfu/ml λ phage particles *in vitro* for 4 days. Then, the splenocytes were collected, washed and immunophenotyped by using the following anti-mouse monoclonal antibodies: CD3-eFluor 450, CD4-FITC (Thermofisher Scientific), and CD8a-APC-H7 (BD Biosciences). Appropriate isotype controls were used for analysis. After staining, the cells were assessed by a BD FACSAria™ II Flow Cytometer (BD Biosciences, San Jose, CA, USA). Dead cells were excluded by using a LIVE/DEAD® Viability Kit (Invitrogen). Antigen specific $CD4^+$ or $CD8^+$ T cells were analyzed with a Flowjo software (Tree Star Inc., Ashland, OR)[9].

Statistical analysis

All statistical analyses were performed using SPSS software (version 22.0). Differences between two groups were evaluated by student's t or Fisher's Exact tests unless otherwise stated. Equality of variance was examined using the F-test. A p value <0.05 (2-tailed) was considered statistically significant.

Results

ASPH mediates resistance to DOX

Proliferating cell nuclear antigen (PCNA), a DNA clamp, acts as a processivity factor for DNA polymerase δ and is essential for replication. The Ki-67 nuclear protein is a cellular marker for proliferation. Cellular content of Ki-67 markedly increases during cell progression through S phase of the cell cycle. Cyclins function as regulators of CDKs (Cyclin-dependent kinase). For example, Cyclin D1, a regulatory subunit of CDK4/CDK6, is required for progression through G1 phase of cell cycle. Cyclin D1 dimerizes with CDK4/6 to regulate G1/S phase transition and entry into S-phase. Cyclin D1 overexpression correlates with early cancer onset and tumor progression. Cyclin D1 spurs oncogenesis by increasing angiogenesis, inducing chemotherapeutic resistance as well as protecting from apoptosis. Cyclin E binds to G1 phase CDK2, which is required for the transition from G1 to S phase of the cell cycle that determines initiation of DNA duplication. Overexpression of cyclin E correlates with tumorigenesis. Firstly, we explored if ASPH could affect sensitivity vs. resistance to DOX in breast cancer. As a result, ASPH generated resistance to DOX mediated cytotoxicity (**Figure 1A-C**) and promoted cell proliferation by upregulating PCNA and Ki67 expression at mRNA and protein levels as measured by qPCR and Western blot, respectively, in MDA-MB-231 (**Figure 1D-I**). Consistently, "KD" of ASPH increased sensitivity to DOX (**Figure 1J-L**) by

downregulating cyclin D1 (cyclin E to a less extent) in SK-BR-3 at mRNA and/or protein levels (**Figure 1M**, **1N**). α-ketoglutarate (α-KG, a substrate of ASPH, acting as a potential stimulator of ASPH enzymatic activity) and a 3rd generation small molecule inhibitor (SMI) [13, 16] of ASPH enzymatic activity (1182) were applied. Interestingly, SMI (1 μM) but not α-KG (50 μM) specifically rescued sensitivity to DOX (3 or 6 μM) in breast cancer cells with endogenous or exogenous ASPH (**Figure 1O-S**). Thus, ASPH enzymatic activity is required for mediating chemoresistance to DOX. Inhibition of ASPH's β-hydroxylase activity may contribute to vulnerability of breast cancer cells to cytotoxicity exerted by DOX.

ASPH inhibits DNA damage response to single- and double-strand breaks and impairs apoptosis induced by DOX

Double-strand breaks (DSBs), in which both strands in the double helix are severed, are particularly hazardous due to genome rearrangements. H_2A histone family member X (H_2AX) contributes to nucleosome-formation, chromatin-remodeling and DNA repair, which is used *in vitro* as an assay for DSBs in dsDNA. Phosphorylated γH_2AX (140S) forms immediately in response to DSBs. Double-strand breaks, in which both strands in the double helix are severed, are particularly hazardous to the cell because they can lead to genome rearrangements. Three machineries are applied to repair double-strand breaks (DSBs): non-homologous end joining (NHEJ), microhomology-mediated end joining (MMEJ), and homologous recombination (HR). We thus examined if ASPH could modify DOX induced DNA damage and repair process in breast cancer.

Accordingly, DSBs were accumulated in response to DOX as demonstrated by a substantial increase in γ-H_2AX in MDA-MB-231 or 4T1 cells with endogenous ASPH, respectively (**Figure 2A**, **2B**). Growth arrest and DNA-damage-inducible protein GADD45A is an indicator of DNA damage, with its transcription upregulated following stressful growth arrest or DNA-damaging agents. GADD45A, an inducer of HR at DSBs, and cleaved PARP1 (Poly (ADP-Ribose) Polymerase 1), as an initiator of single-stand breaks (SSBs) repair, were induced at early (at 1 h after treatment) vs. late (at 4-8 h) stage in response to DOX (**Figure 2C**, **2D**).

Genome instability is a hallmark of cancer, which is accelerated by defects in cellular responses to DNA damage. Through interacting with components, MRE11-RAD50-NBS1 (MRN) complex plays a crucial role in sensing and repair of DNA damage. As a sensor for DNA damage (DSBs) induced by DOX, MRE11, RAD50 and NBS1 were phosphorylated and formed an active MRN complex in MDA-MB-231 Vector cells with endogenous ASPH. In contrast, this active form of MRN complex was not active in the presence of exogenous ASPH (**Figure 2E-G**). Active MRN complex recruited ATM (ataxia-telangiectasia mutated kinase) with endogenous ASPH, which was subsequently activated and thus activated (phosphorylated) P53 through HIPK2 (homeodomain interacting protein kinase 2) and AMPK (5' adenosine monophosphate-activated protein kinase) (**Figure 2H-P**).

Exogenous ASPH attenuated genomic lesions as a net effect. ASPH suppressed sensors and executors for error-free DSBs repair system (e.g., HR [17]) or SSBs repair system (**Figure 3A**, **3B**). When ASPH was knocked-down, as a net effect, γ-H_2AX were accumulated gradually and substantially due to reduced DSBs repair (**Figure 3A-D**). GADD45A, an inducer of HR at DSBs, and cleaved PARP1, as an initiator of SSBs repair, were induced at early (at 1 h after treatment) vs. late (at 4-8 h) stage in response to DOX. The active MRN complex was recovered when ASPH was knocked-down in SK-BR-3 cells (**Figure 3A**, **3E-G**). This pattern was inhibited by exogenous high levels of ASPH. "KD" of ASPH recovered this MRN complex-ATM-P53 cascade (**Figure 3A**, **3H-K**). HRK (activator of apoptosis hara-kiri) regulates apoptosis through interaction with death-repressor proteins Bcl-2 and Bcl-X(L). BIM (Bcl-2-like protein 11) interacts with BCL2, BCL2L1/BCL-X(L) and MCL1, to act as an apoptotic activator. In the presence of endogenous ASPH, this cascade could also induce apoptosis as demonstrated by upregulation of cleaved caspase-3, HRK and BIM (**Figure 3L-Q**).

By contrast, downregulation of major pro-apoptotic components and upregulation of anti-apoptotic elements were mediated by endogenous or exogenous high levels of ASPH (**Figure 4A-G**). Accordingly, "KD" of ASPH rescued pro-apoptotic pattern in SK-BR-3 cells (**Figure 4H-L**). Therefore, ASPH mediated resistance to

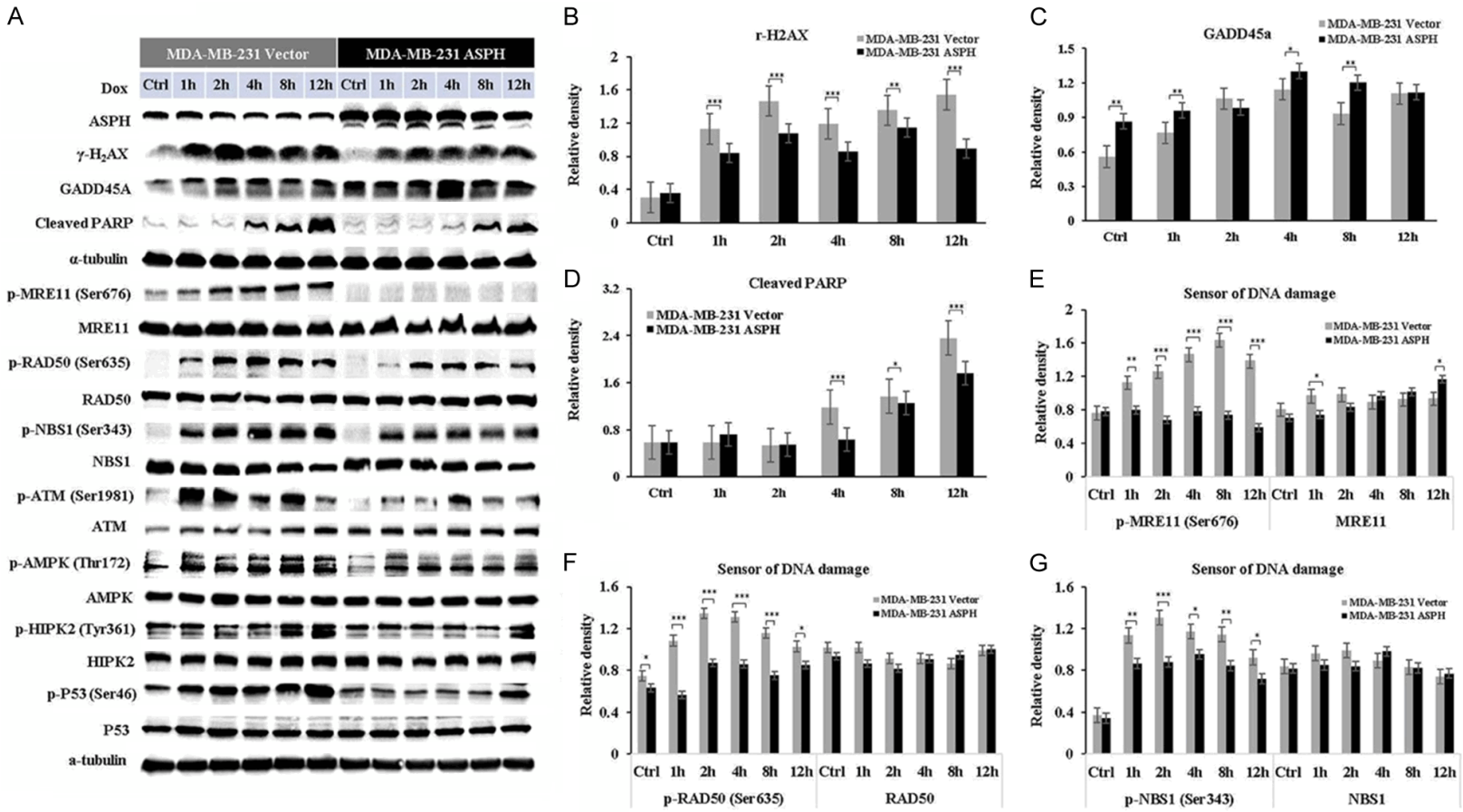
A
MDA-MB-231 Vector
MDA-MB-231 ASPH
Dox
Ctrl 1h 2h 4h 8h 12h Ctrl 1h 2h 4h 8h 12h
ASPH
γ-H2AX
GADD45A
Cleaved PARP
α-tubulin
p-MRE11 (Ser676)
MRE11
p-RAD50 (Ser635)
RAD50
p-NBS1 (Ser343)
NBS1
p-ATM (Ser1981)
ATM
p-AMPK (Thr172)
AMPK
p-HIPK2 (Tyr361)
HIPK2
p-P53 (Ser46)
P53
a-tubulin
B
r-H2AX
MDA-MB-231 Vector
MDA-MB-231 ASPH
Relative density
Ctrl 1h 2h 4h 8h 12h
C
GADD45a
D
Cleaved PARP
E
Sensor of DNA damage
p-MRE11 (Ser676)
MRE11
F
Sensor of DNA damage
p-RAD50 (Ser635)
RAD50
G
Sensor of DNA damage
p-NBS1 (Ser343)
NBS1

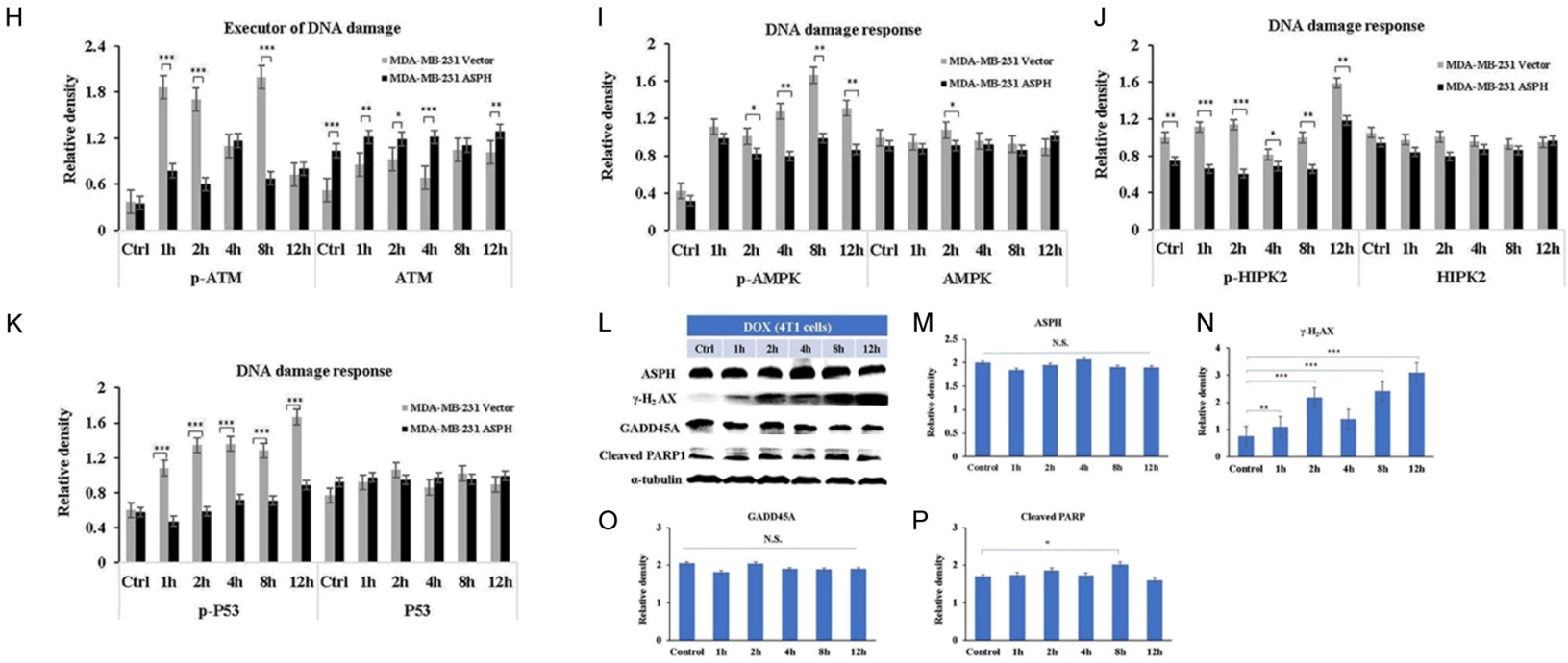

Figure 2. ASPH mediates resistance to doxorubicin induced DNA damage response. (A) ASPH downregulates major components of error-free DNA damage repair machinery in response to DOX, including sensors and executors of DNA DSB or SSB repair system (e.g., HR). ASPH results in collapse of active/functional MRN complex and renders anti-apoptosis. (B-K) Quantification of dynamic changes in expression profiling of components in (A). (L) Biomarkers for DOX induced DNA damage response in 4T1. (M-P) Quantification of elements expression in (L). $^{*}P<0.05$; $^{**}P<0.01$; $^{***}P<0.001$ compared to corresponding control. Data were expressed as mean ± SD calculated from each experiment performed in triplicate under each condition.

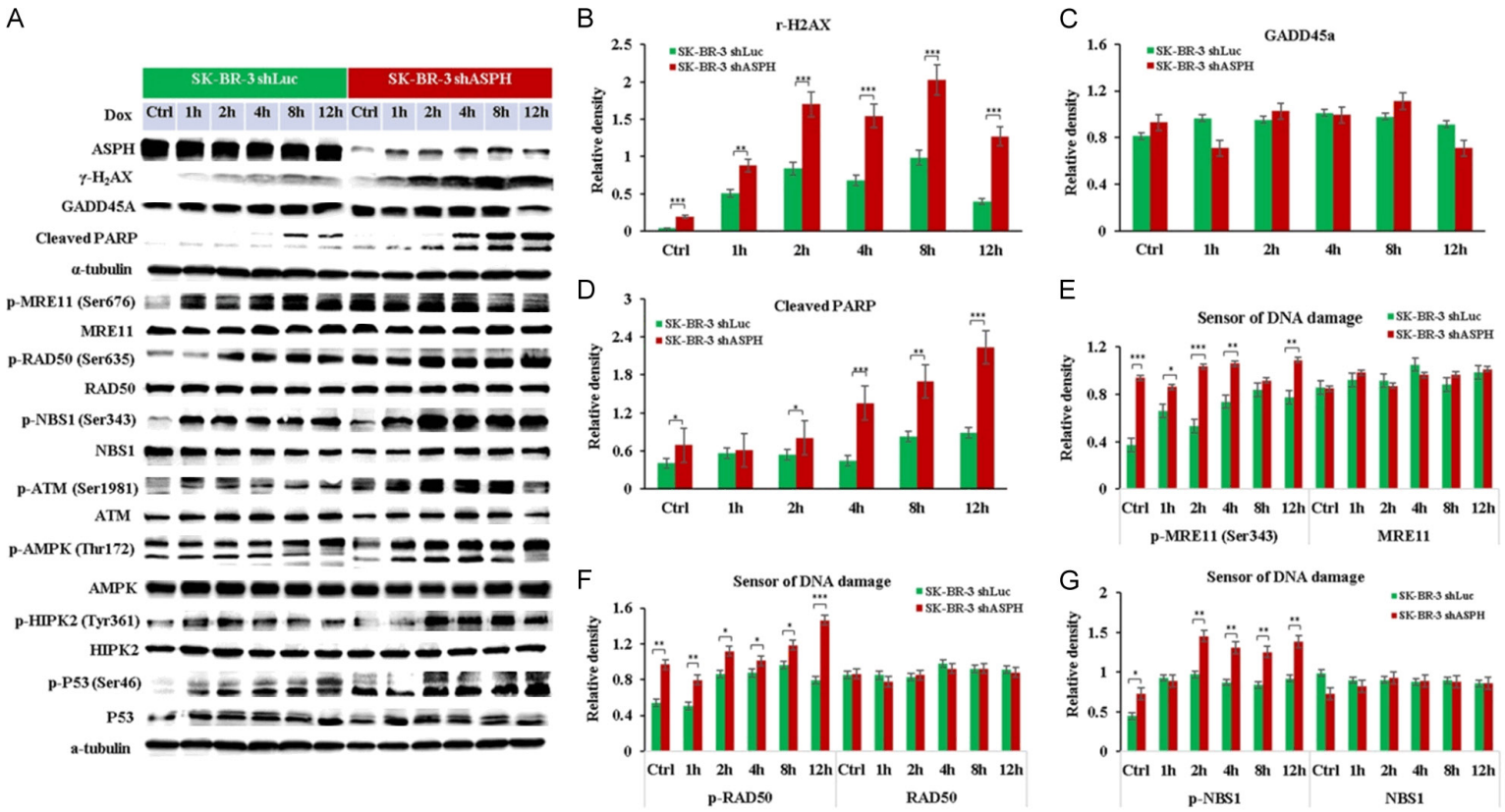
A
SK-BR-3 shLuc
SK-BR-3 shASPH
Dox
Ctrl 1h 2h 4h 8h 12h Ctrl 1h 2h 4h 8h 12h
ASPH
γ-H2AX
GADD45A
Cleaved PARP
α-tubulin
p-MRE11 (Ser676)
MRE11
p-RAD50 (Ser635)
RAD50
p-NBS1 (Ser343)
NBS1
p-ATM (Ser1981)
ATM
p-AMPK (Thr172)
AMPK
p-HIPK2 (Tyr361)
HIPK2
p-P53 (Ser46)
P53
a-tubulin
B
r-H2AX
SK-BR-3 shLuc
SK-BR-3 shASPH
Relative density
Ctrl 1h 2h 4h 8h 12h
C
GADD45a
D
Cleaved PARP
E
Sensor of DNA damage
p-MRE11 (Ser343)
MRE11
F
Sensor of DNA damage
p-RAD50
RAD50
G
Sensor of DNA damage
p-NBS1
NBS1

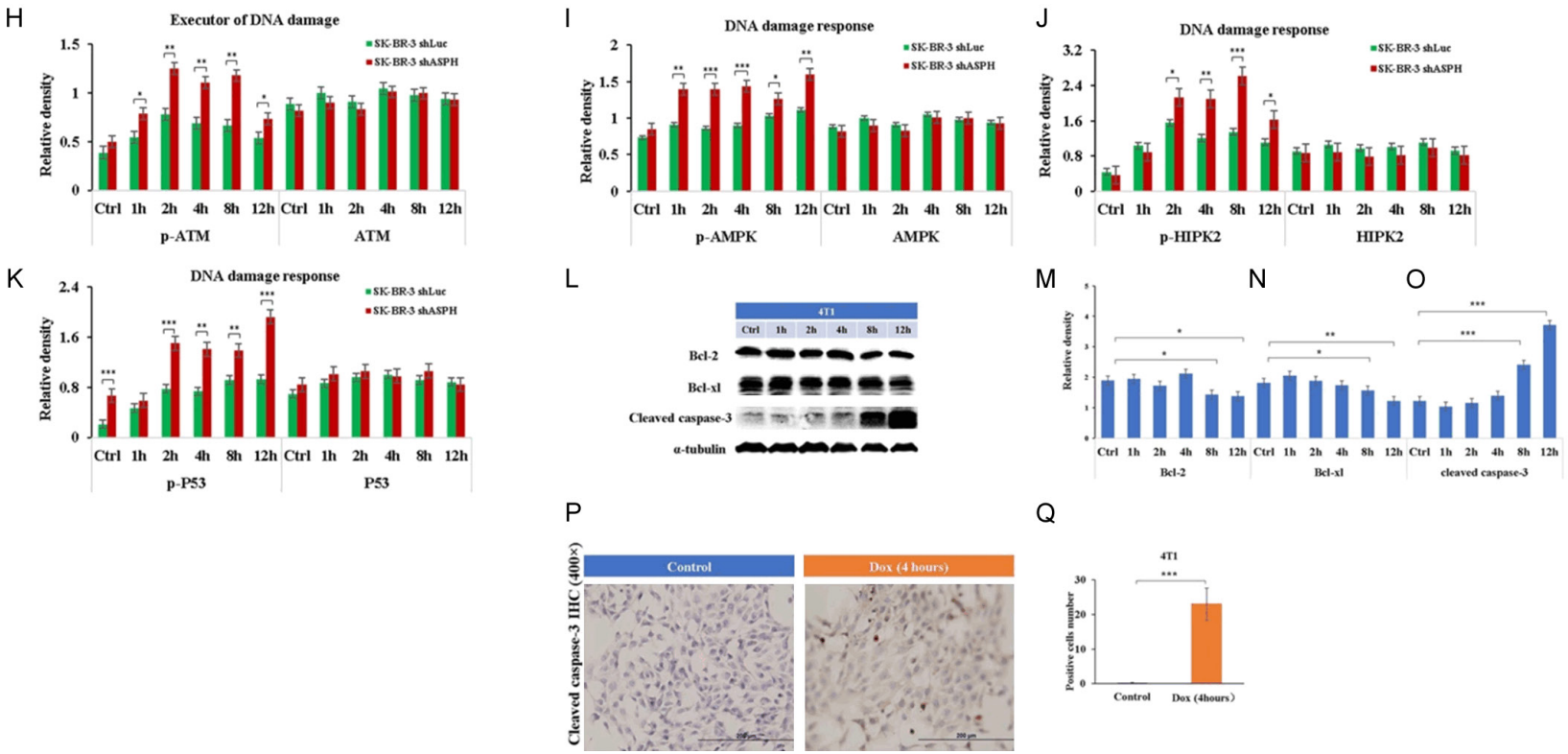

Figure 3. ASPH mediates resistance to doxorubicin induced DNA damage response in SK-BR-3 cells. (A) ASPH downregulates major components of error-free DNA damage repair machinery in response to DOX, including sensors and executors of DNA DSB or SSB repair system (e.g., homologous recombination). ASPH causes collapse of active/functional MRN complex and renders anti-apoptosis. This inhibition is reversed by ASPH knocking-down. (B-K) Quantification of dynamic changes in expression profiling of components in (A). (L-O) Dynamic changes in expression profiling of major components involved in apoptosis in response to DOX in 4T1. (P, Q) Upregulation of cleaved caspase-3 overtime in response to DOX as measured by IHC in 4T1. $^{*}P<0.05$; $^{**}P<0.01$; $^{***}P<0.001$ compared to corresponding control. Data were expressed as mean ± SD calculated from each experiment performed in triplicate under each condition.

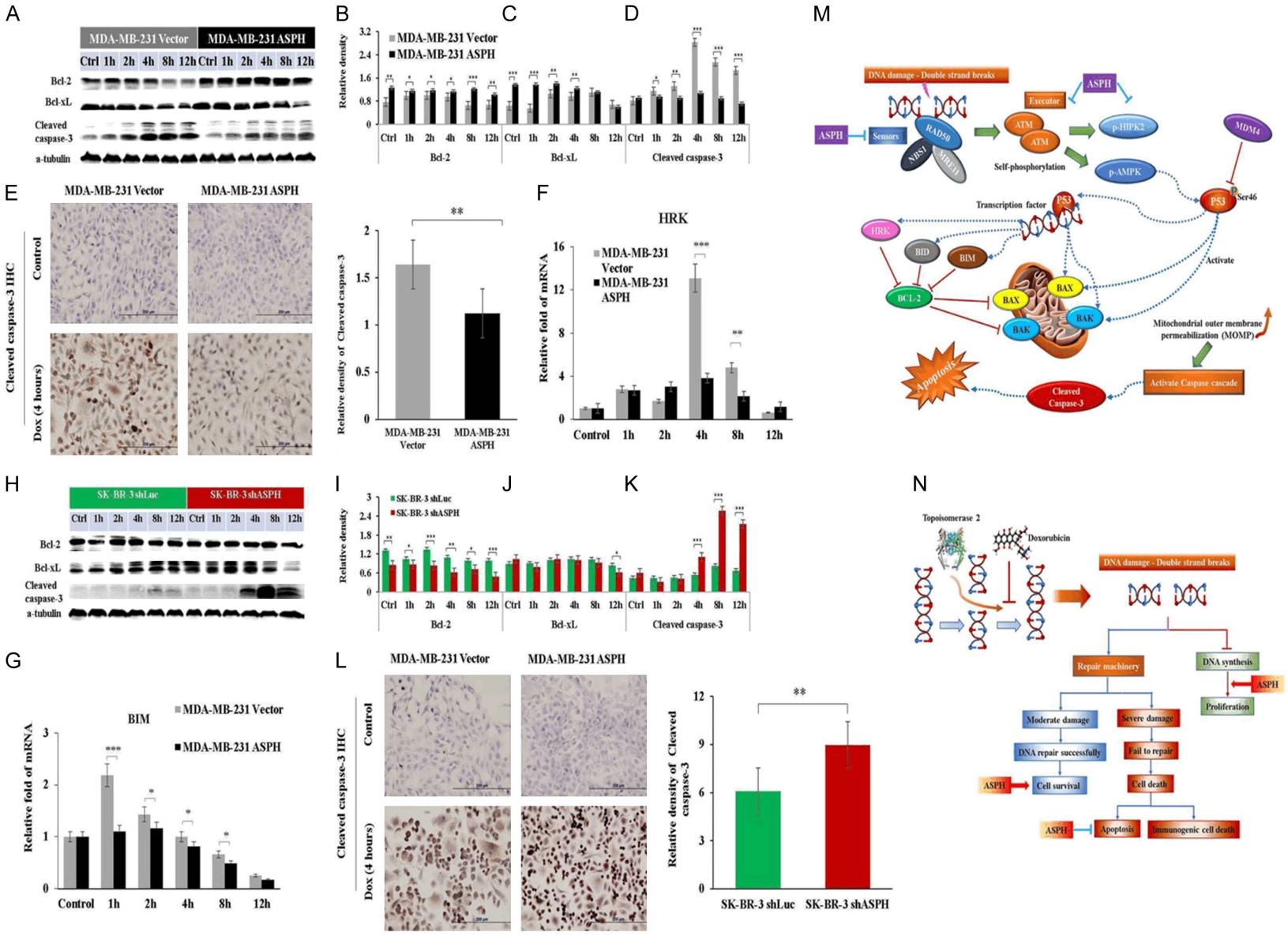
A
MDA-MB-231 Vector
MDA-MB-231 ASPH
Ctrl 1h 2h 4h 8h 12h Ctrl 1h 2h 4h 8h 12h
Bcl-2
Bcl-xL
Cleaved caspase-3
a-tubulin
B
C
D
Relative density
MDA-MB-231 Vector
MDA-MB-231 ASPH
Bcl-2
Bcl-xL
Cleaved caspase-3
M
DNA damage - Double strand breaks
Executor
ASPH
Sensors
RAD50
NBS1
MRE11
ATM
ATM
p-HIPK2
p-AMPK
Self-phosphorylation
MDM4
P53
Ser46
Transcription factor
HRK
BID
BIM
BCL-2
BAX
BAX
BAK
BAK
Activate
Mitochondrial outer membrane permeabilization (MOMP)
Apoptosis
Cleaved Caspase-3
Activate Caspase cascade
E
MDA-MB-231 Vector
MDA-MB-231 ASPH
Cleaved caspase-3 IHC
Control
Dox (4 hours)
Relative density of Cleaved caspase-3
MDA-MB-231 Vector
MDA-MB-231 ASPH
F
HRK
MDA-MB-231 Vector
MDA-MB-231 ASPH
Relative fold of mRNA
Control 1h 2h 4h 8h 12h
H
SK-BR-3 shLuc
SK-BR-3 shASPH
Ctrl 1h 2h 4h 8h 12h Ctrl 1h 2h 4h 8h 12h
Bcl-2
Bcl-xL
Cleaved caspase-3
a-tubulin
I
J
K
Relative density
SK-BR-3 shLuc
SK-BR-3 shASPH
Bcl-2
Bcl-xL
Cleaved caspase-3
N
Topoisomerase 2
Doxorubicin
DNA damage - Double strand breaks
Repair machinery
DNA synthesis
ASPH
Proliferation
Moderate damage
Severe damage
DNA repair successfully
Fail to repair
ASPH
Cell survival
Cell death
ASPH
Apoptosis
Immunogenic cell death
G
BIM
MDA-MB-231 Vector
MDA-MB-231 ASPH
Relative fold of mRNA
Control 1h 2h 4h 8h 12h
L
MDA-MB-231 Vector
MDA-MB-231 ASPH
Cleaved caspase-3 IHC
Control
Dox (4 hours)
Relative density of Cleaved caspase-3
SK-BR-3 shLuc
SK-BR-3 shASPH

Figure 4. ASPH mediates anti-apoptosis in response to doxorubicin. A-L. Anti-apoptotic (BCL-2 and BCL-XL) components are upregulated, whereas pro-apoptotic (HRK, cleaved caspase-3 and BIM) are downregulated at mRNA and/or protein levels by ASPH at early stage in response to DOX. E, L. Pro-apoptotic cleaved caspase-3 is downregulated by ASPH, which is reversed by ASPH knocking-down as measured by IHC. M, N. Hypothetic role of ASPH in doxorubicin induced DNA damage response and apoptosis in breast cancer. M. Cellular response to DNA double strand breaks (DSBs) caused by doxorubicin in breast cancer cells highly expressing ASPH. N. Cellular phenotypic consequences of doxorubicin therapy are multifacetedly distorted by ASPH as a mechanism of drug-resistance. This scenario is expected to be substantially reversed when ASPH's oncogenic property is inhibited/blocked, which may convert breast cancer cells from survival to death. $^{*}P<0.05$; $^{**}P<0.01$; $^{***}P<0.001$; $^{****}P<0.0001$ compared to corresponding control. Data were expressed as mean ± SD calculated from each experiment performed in triplicate under each condition.

DOX by fostering proliferation and survival and impeding apoptosis (**Figure 4M**, **4N**).

Immunogenic cell death (ICD) induced by DOX

ICD/immunogenic apoptosis is characterized by apoptotic morphology, maintenance of membrane integrity, resulting in a regulated activation of host immune response. Endoplasmic reticulum (ER) stress is generally recognized as a causative agent for ICD, with high production of reactive oxygen species (ROS). We explored if ASPH could be involved in regulating DOX-induced ICD in breast cancer.

Calreticulin is a multifunctional soluble protein that binds Ca^{2+} ions (a second messenger in signal transduction), rendering it inactive. Calreticulin binds to misfolded proteins and inhibits their export from endoplasmic reticulum to Golgi apparatus. Eukaryotic translation initiation factor 2 subunit 1 (eIF2α) catalyzes an early regulated step of protein synthesis initiation. Phosphorylation of eIF2α triggers cytochrome c release from mitochondria during apoptosis. Extracellular high-mobility group box1 (HMGB1) functions as prototypical alarmin to activate innate immunity, upon actively released from cells or passively released upon cell death. Toll-like receptor 4 (TLR4) and receptor for advanced glycation endproducts (RAGE) operate as the main HMGB1 receptors.

In response to DOX induced DNA damage, eIF2α was phosphorylated and upregulated to initiate ICD in dying DOX sensitive cancer cells with endogenous ASPH (**Figure 5A**, **5B**). The level of p-eIF2α reached peak at 8 h in cells with low endogenous ASPH vs. at 12 h (delayed) in cells with high exogenous ASPH. This active eIF2α intensified dying cells to secrete damage-associated molecular patterns (DAMPs), such as calreticulin (CALR), ATP and HMGB1 (**Figure 5C-E**). Secreted HMGB1 was identified by ELISA using supernatant from cell culture (**Figure 5K-M**). The expression of DAMPs from cell lysate was induced by exogenous or endogenous ASPH in DOX sensitive cells; whereas reduced or delayed by "KD" of ASPH (**Figure 5F-J**, **5L**, **5M**). The expression of acetylated HMGB1 reached peak at 2 h in cells with endogenous high ASPH vs. at 12 h (delayed) in cells with ASPH KD cells. The release of HMGB1 was induced by high ASPH and accordingly, reduced by ASPH-KD.

Combinatory therapy inhibits primary mammary tumor growth and pulmonary metastases in orthotopic xenograft murine models

To explore if immunotherapy targeting ASPH antigen either alone or in combination with chemotherapy could suppress tumor development and progression, an orthotopic xenograft murine model of breast cancer using 4T1 was established in immunocompetent BALB/c mice (**Figure 6A**). Compared to control group, primary mammary tumor growth was suppressed to the most extent by combinatory therapy (DOX+Vaccine), followed by DOX or Vaccine alone (**Figure 6B-F**). The 4T1 cells with highly aggressive and invasive capability rapidly generated multiple pulmonary metastases in BALB/c mice. Pulmonary metastases were identified at a high frequency (**Figure 6G**). Other common metastatic sites include liver, adrenal glands, kidney, and lymph nodes. Importantly, combined application of DOX and vaccine produced the highest suppression rate on pulmonary metastases, followed by Vaccine or DOX alone (**Figure 6H**, **6I**). Histopathological characteristics of these tumors demonstrated densely arrangement with high-grade nuclear atypia, and a high-index of ASPH expression in both primary and metastatic lesions (**Figure 6J**, **6K**). Notably, lymphatic metastases were observed adjacent to the right iliac vessel system (**Figure 7A**, **7B**), which was substantially attenuated by Vaccine or combinatory therapy (**Figure 7C**).

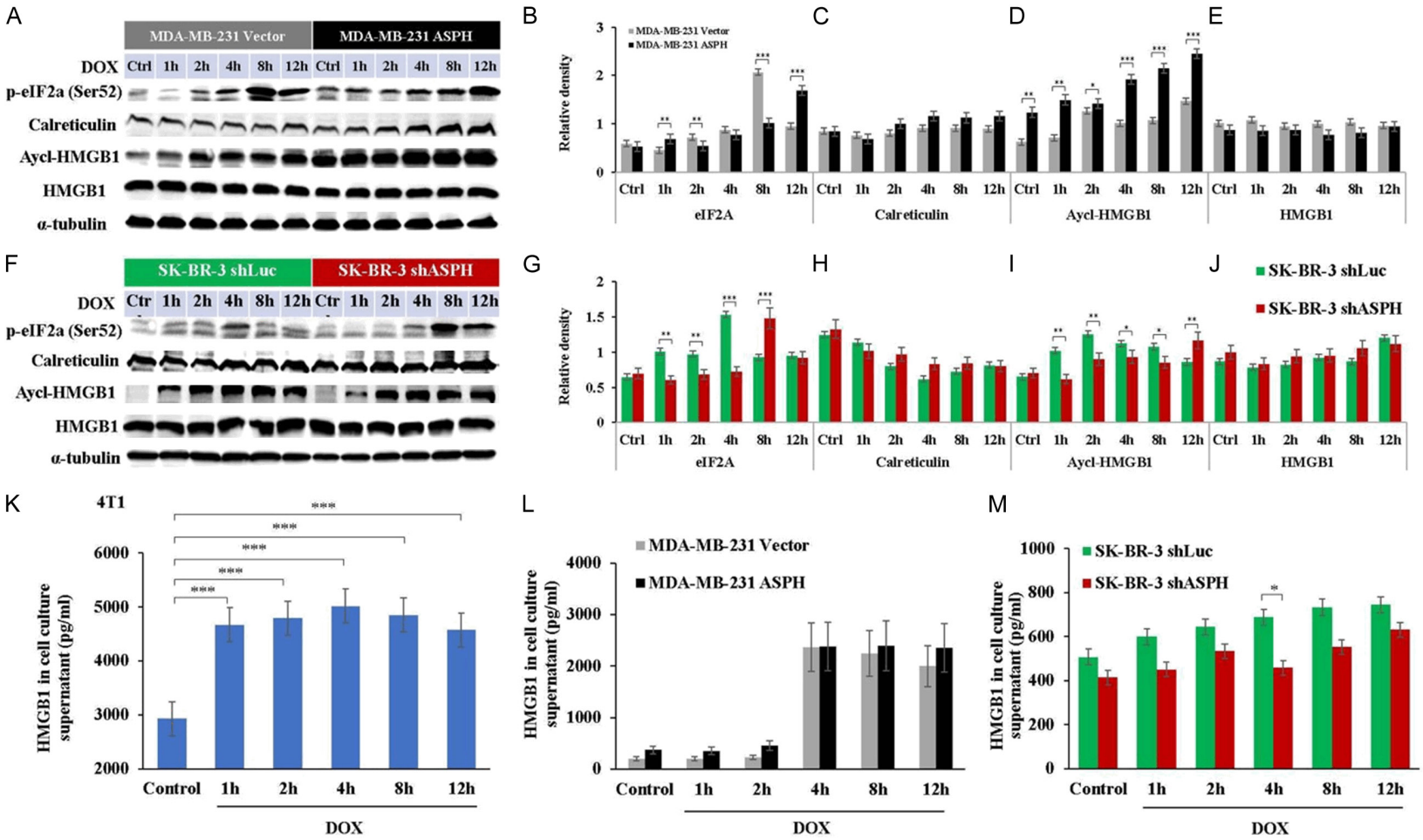

Figure 5. ASPH mediates resistance to doxorubicin induced immunogenic cell death (ICD). A-J. Dynamic changes in expression profiling of ER stress marker (p-eIF2α), Eat me signal calreticulin (CALR) and a ligand (HMGB1) on cancer cells of TLR4 receptor on DCs in response to DOX in MDA-MB-231 or SK-BR-3 cells. K-M. Release of HMGB1 into condition medium by different breast cancer cells in response to DOX. $^{*}P<0.05$; $^{**}P<0.01$; $^{***}P<0.001$; $^{****}P<0.0001$ compared to corresponding control. Data were expressed as mean ± SD calculated from each experiment performed in triplicate under each condition.

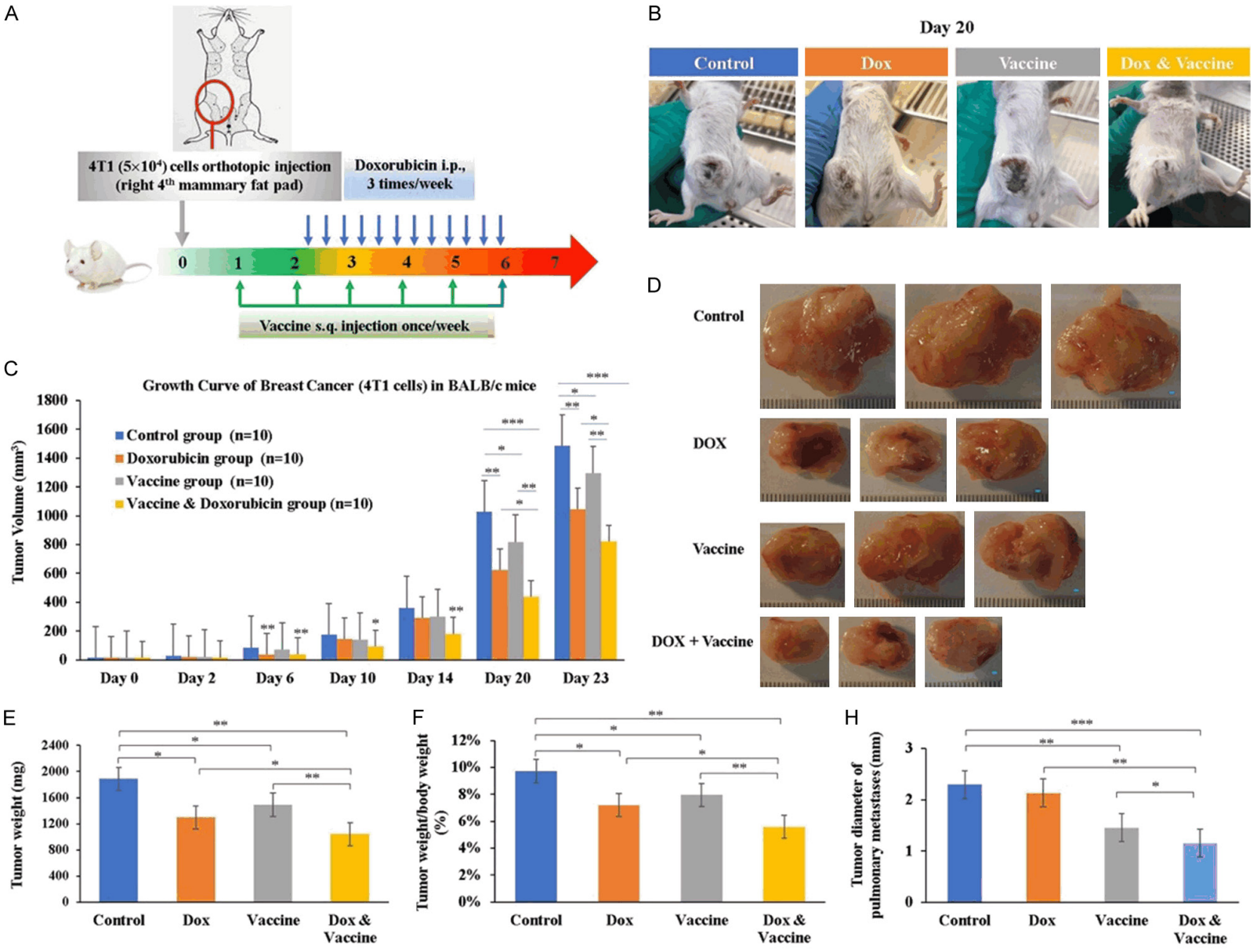
A
4T1 (5×10⁴) cells orthotopic injection (right 4th mammary fat pad)
Doxorubicin i.p., 3 times/week
0 1 2 3 4 5 6 7
Vaccine s.q. injection once/week
B
Day 20
Control
Dox
Vaccine
Dox & Vaccine
C
Growth Curve of Breast Cancer (4T1 cells) in BALB/c mice
Tumor Volume (mm³)
Control group (n=10)
Doxorubicin group (n=10)
Vaccine group (n=10)
Vaccine & Doxorubicin group (n=10)
Day 0 Day 2 Day 6 Day 10 Day 14 Day 20 Day 23
D
Control
DOX
Vaccine
DOX + Vaccine
E
Tumor weight (mg)
Control Dox Vaccine Dox & Vaccine
F
Tumor weight/body weight (%)
Control Dox Vaccine Dox & Vaccine
H
Tumor diameter of pulmonary metastases (mm)
Control Dox Vaccine Dox & Vaccine

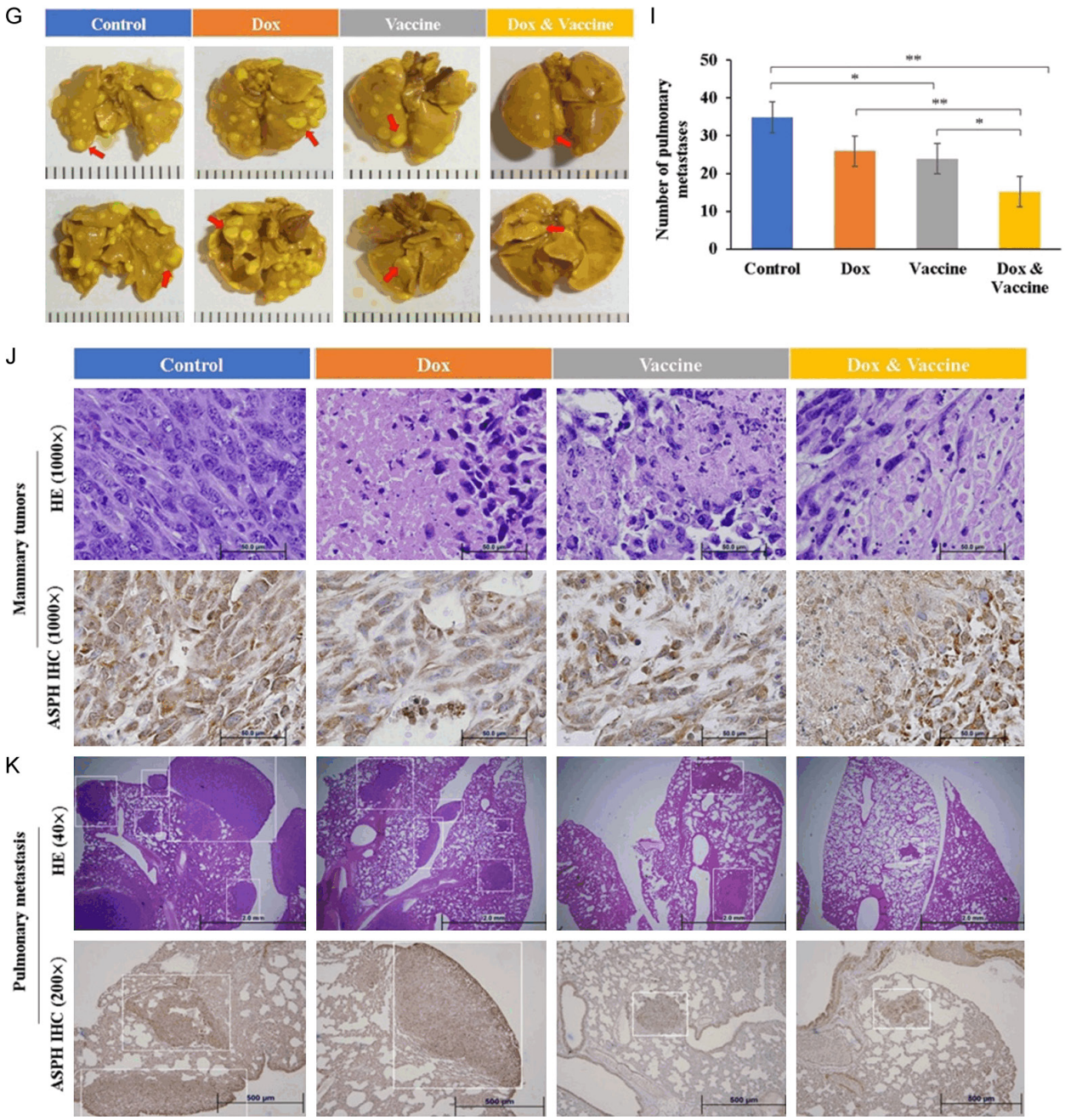

Figure 6. Synergistic antitumor effects of doxorubicin combined with ASPH-based λ phage vaccine in an orthotopic murine breast cancer model. A. Scheme for establishing an orthotopic breast cancer model using BALB/c mice. Animals were randomly divided into 4 groups (n=10 mice per group). B. Gross appearance of mammary lesions in represented mice from different experimental groups. C. Tumor volume in mice from different groups. D. Gross appearance of primary mammary tumors in represented mice from different groups. Scale bar, 1 mm. E. Tumor weight of mice from different groups. F. Ratio of tumor weight vs. body weight of mice from different groups. G. Gross appearance of involved lungs of represented mice from different groups. H. Maximum diameters of macro-metastatic pulmonary lesions of mice from different groups. I. Number of macro-metastatic pulmonary lesions of mice from different groups. J, K. Histology features and ASPH expression patterns of primary mammary tumors and pulmonary metastases in represented mice from different groups. $^{*}P<0.05$; $^{**}P<0.01$; $^{***}P<0.001$; $^{****}P<0.0001$ compared to corresponding control (Student's t-test). Data are presented as mean ± SD calculated from each experiment performed in triplicate under each condition.

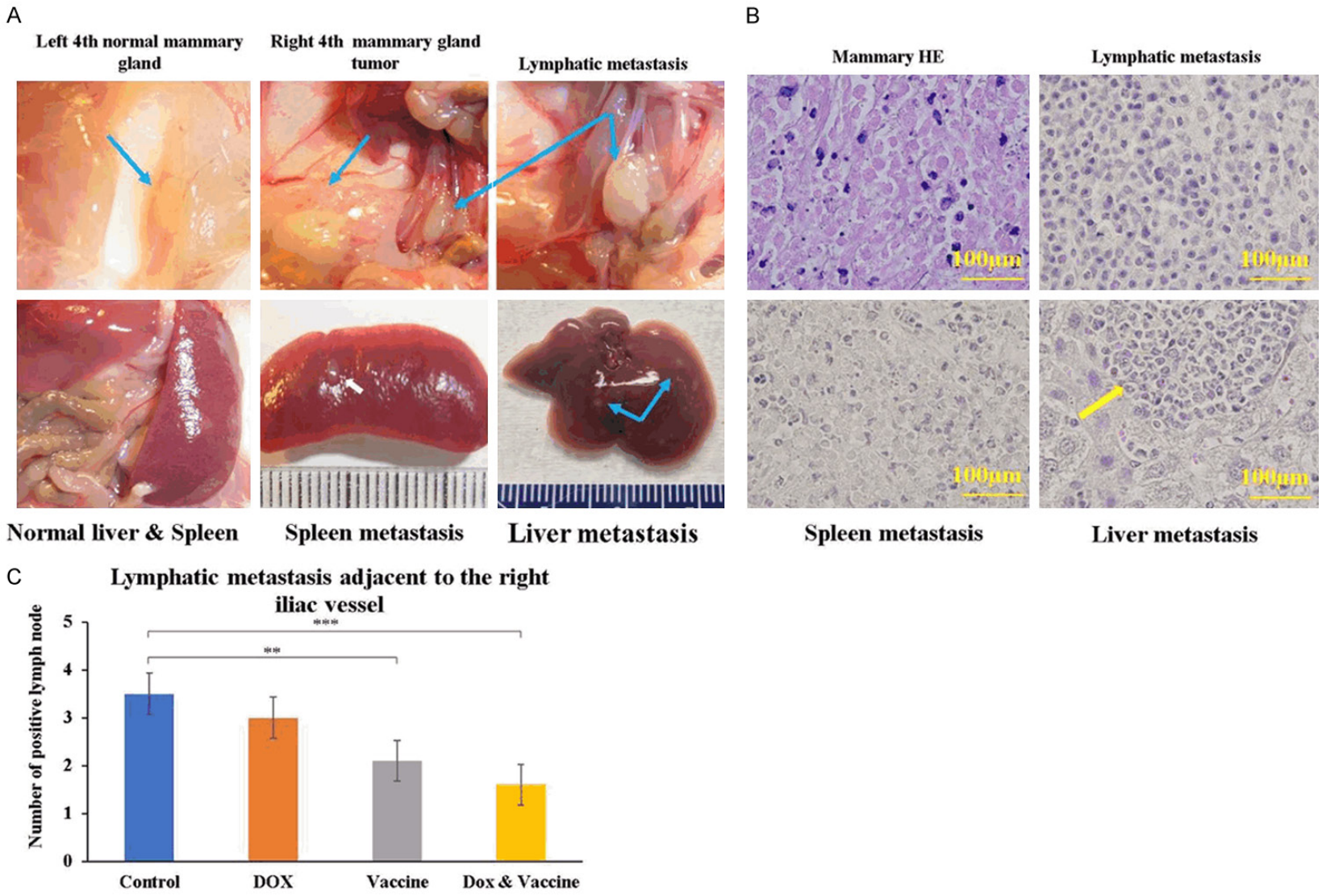

Figure 7. Multi-organ metastasis of a murine model of breast cancer. (A) Gross appearance of primary and metastatic tumors in various organs from control group. (B) Histology features of (A). (C) Lymphatic metastasis in different groups. $^{*}P<0.05$; $^{**}P<0.01$; $^{***}P<0.001$ compared to corresponding control (Student's t-test). Data are presented as mean ± SD calculated from each experiment performed in triplicate under each condition.

Combinatory therapy inhibits proliferation and promotes apoptosis in vivo

We next explored if ASPH axis mediated resistance to DOX could be reversed by immunotherapy targeting ASPH antigen. The accumulation of γ-H_2AX was increased to the most extent in response to DOX, followed by Vaccine alone or combination treatment. GADD45A and cleaved PARP1 were upregulated in response to DOX or combination treatment (**Figure 8A**). Blockade of tumor growth was attributed to reduced proliferation, as demonstrated by downregulated PCNA, cyclin D1 and cyclin E (**Figure 8B**); and boosted apoptosis, as clarified by upregulated pro-apoptotic cleaved caspase-3, downregulated anti-apoptotic BCL-XL and BCL-2 (**Figure 8C**), as well as increased number of dead cells, as quantified by immunofluorescent and TUNEL staining (**Figure 8D**, **8E**).

Combinatory therapy induces ICD in vivo

We further tested if immunotherapy targeting ASPH antigen could rescue and even enhance DOX induced ICD. Combinatory therapy substantially enhanced ICD as highlighted by upregulation of p-eIF2A, CALR and HMGB1 in tumor tissues (**Figure 9A**, **9B**). Subcellular localization of active eIF2A in nucleus (**Figure 9C**, **9D**) promoted translation initiation of CALR (**Figure 9E**, **9F**) and HMGB1 (**Figure 9G**). Exposure of "eat me" signal CALR on the surface in both primary mammary tumors and pulmonary metastatic lesions and augmented serum levels of HMGB1 (**Figure 9H**) promoted ICD as further clarified by substantially elevated levels of serum INFγ (**Figure 9I**). The level of INFγ was enhanced up to 2323 pg/ml (3.27-fold increase than control) in response to combinatory therapy.

Combinatory therapy magnifies anti-cancer immune response in vivo

Finally, we validated molecular mechanisms underlying how immunotherapy targeting ASPH antigen could reinvigorate host anti-tumor response. Combinatory therapy successfully magnified anticancer immune response as elucidated by in vitro cytotoxicity assay (**Figure 10A**). Compared to control group, lymphocytes (containing CTLs) of mice from Vaccine group efficiently killed 4T1 cells when co-cultured at a ratio of 20:1 (**Figure 10B**). After immunized with ASPH-based λ phage vaccine for 4-8 weeks, cytotoxicity of lymphocytes was further amplified (1.11% vs. 43.9%).

LRP1 is ER chaperone-sensing pattern recognition receptors (PRRs) expressed by antigen-presenting cells such as dendritic cells (DCs). The LRP1 mediates endocytosis of CALR and promotes the engulfment of cellular corpses and debris. Mechanically, combinatory therapy boosted antigen uptake and maturation of DCs by upregulating PRRs such as LRP1 (LDL receptor related protein 1; a receptor for CALR) and TLR4 (a receptor for HMGB1) in primary mammary tumors and pulmonary metastases (**Figure 10C**). Thus, increased CALR-LRP1 and HMGB1-TLR4 interactions between tumor cells and DCs prompted $CD3^+$ T cell recruitment (tumor infiltrated lymphocytes [TILs]) and priming (**Figure 10D**).

ASPH-based λ vaccine supported DCs maturation in secondary lymphatic tissues such as the spleen (**Figure 11A**). Combinatory therapy also efficiently recruited maturated DC and TILs to pulmonary metastatic lesions (**Figure 11B**). Consequently, clonal expansion of T cells led to tumor lysis attributed to effector $CD4^+$ Th1 and $CD8^+$ CTLs (**Figure 11C**, **11D**).

Colony stimulating factor 1 receptor (CSF1R)/macrophage colony-stimulating factor receptor (M-CSFR), a tyrosine kinase transmembrane protein, acts as the receptor for colony stimulating factor 1 (CSF1), a cytokine that controls the production, differentiation, and function of macrophages. CSF1R is overexpressed in many cancers and on tumor-associated macrophages (TAM). Importantly, in the control group, ASPH overexpression on the surface of tumor cells in primary mammary growth may have been protected from immune system attack by recruiting immunosuppressive $CSF1R^+$ type 2 macrophage (M2) in tumor microenvironment as a physical barrier to DCs and TILs (no $CD3^+$ TILs could be detected). By contrast, in the combinatory group, TILs were infiltrated into tumors when no M2 barrier existed (**Figure 12A**, **12B**).

Discussion

In breast cancer, a high level of ASPH mediates resistance to DOX by stimulating cell proliferation and inhibiting DNA damage response

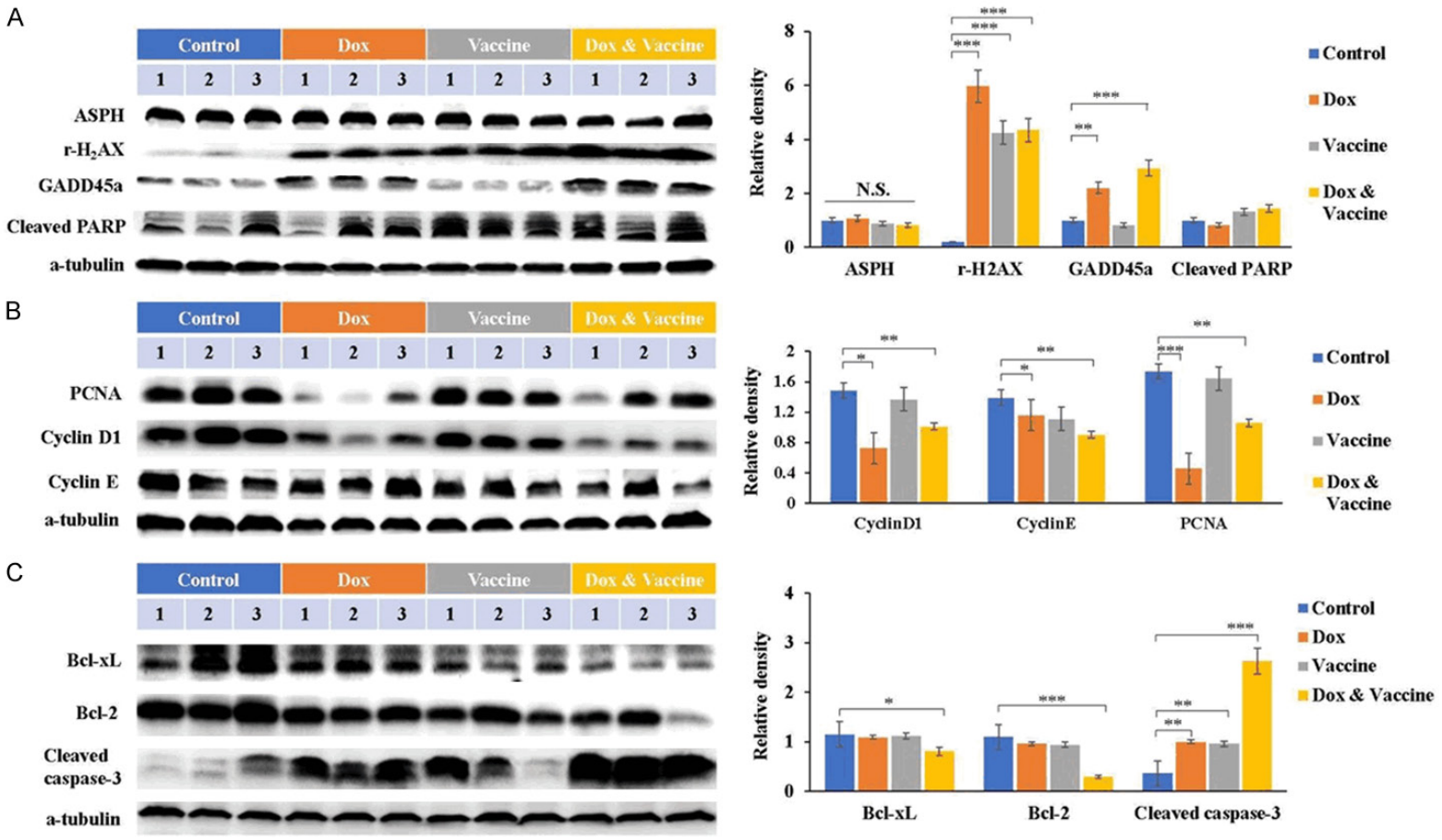
A
Control
Dox
Vaccine
Dox & Vaccine
1 2 3 1 2 3 1 2 3 1 2 3
ASPH
r-H2AX
GADD45a
Cleaved PARP
a-tubulin
Relative density
N.S.
ASPH
r-H2AX
GADD45a
Cleaved PARP
Control
Dox
Vaccine
Dox & Vaccine
B
PCNA
Cyclin D1
Cyclin E
a-tubulin
CyclinD1
CyclinE
PCNA
C
Bcl-xL
Bcl-2
Cleaved caspase-3
a-tubulin

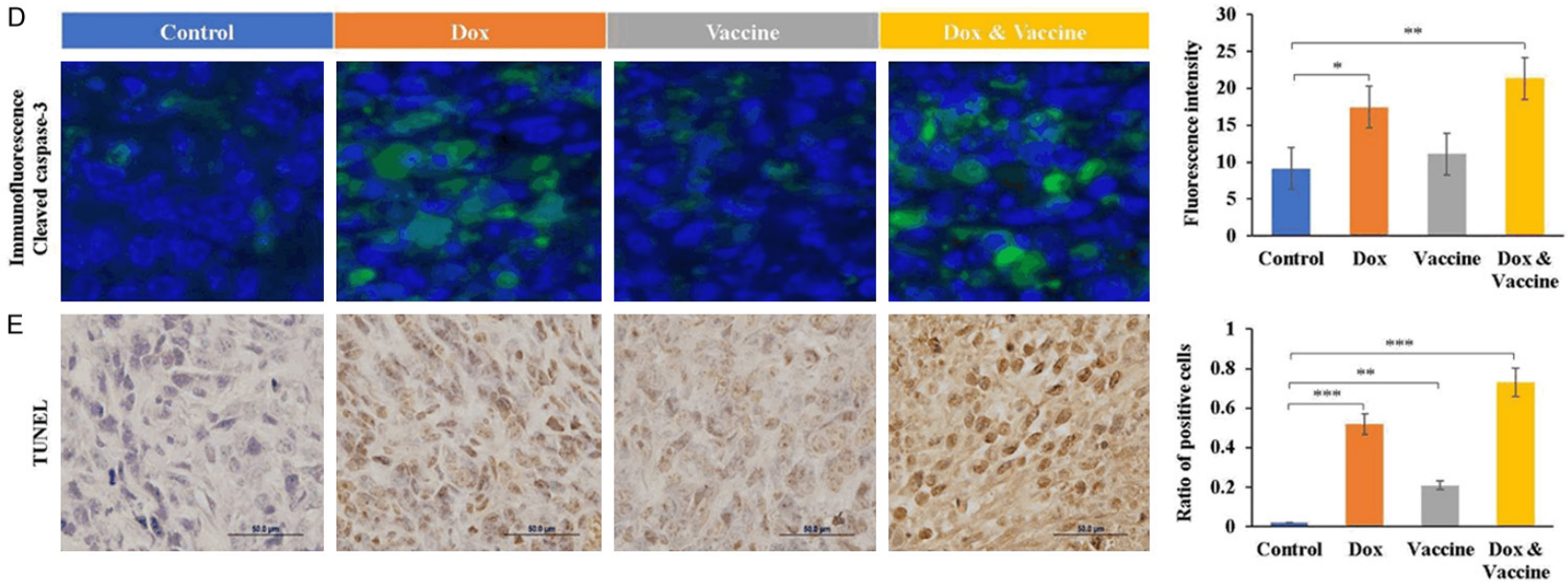

Figure 8. Dynamic changes in expression profiling of major components involved in DNA damage (DSB and SSB) response, proliferation and apoptosis in tumor tissues in representative mice from different groups. A. Expression profiling of elements involved in DSB and SSB repair pathways. B. Expression profiling of proliferation markers. C. Expression profiling of pro- and anti-apoptotic factors. D. Expression of cleaved caspase-3 by IF. E. Apoptosis of tumor cells in mice from different groups. $^{*}P<0.05$; $^{**}P<0.01$; $^{***}P<0.001$; $^{****}P<0.0001$ compared to corresponding control. Data were expressed as mean ± SD calculated from each experiment performed in triplicate under each condition.

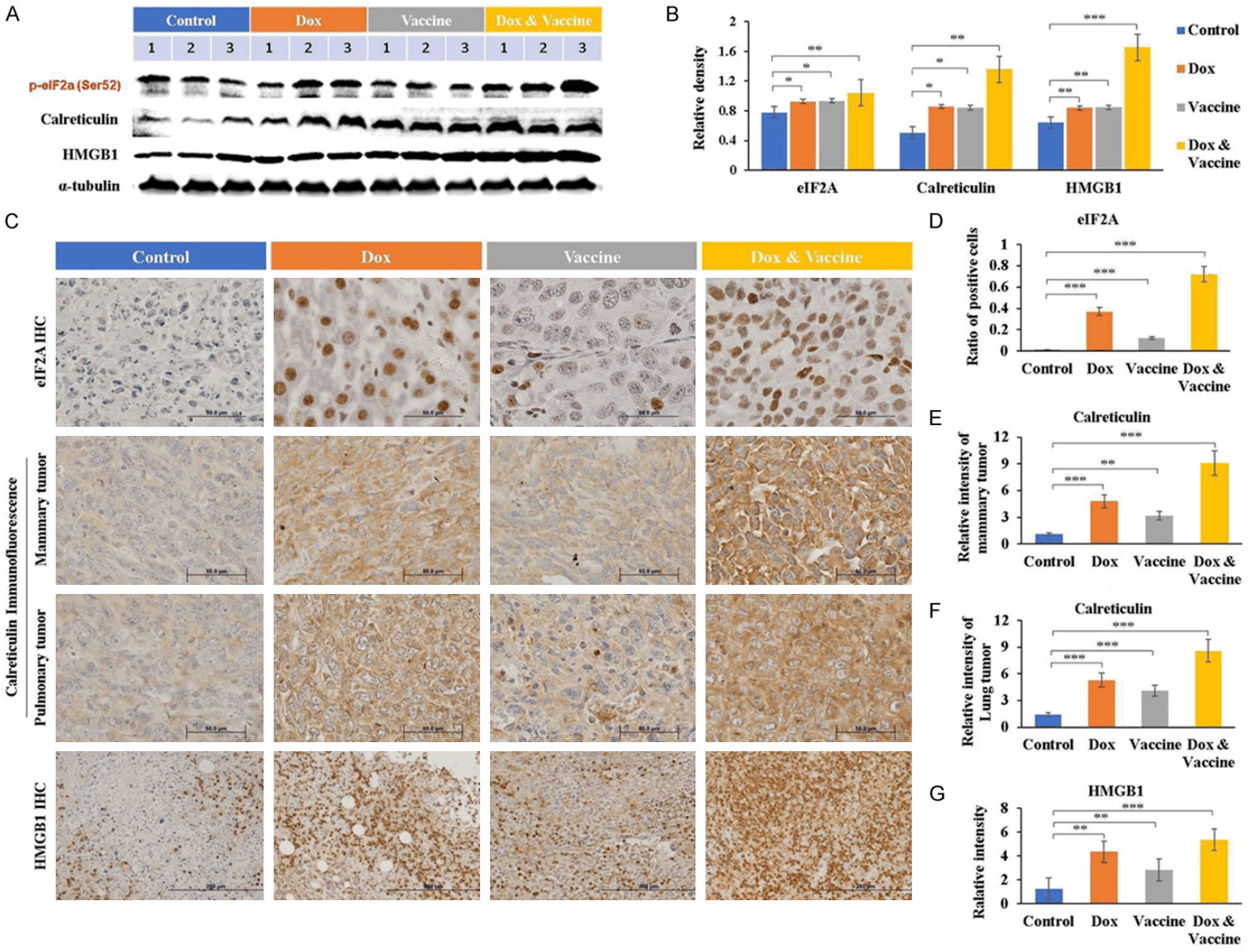
A
Control
Dox
Vaccine
Dox & Vaccine
1 2 3 1 2 3 1 2 3 1 2 3
p-eIF2a (Ser52)
Calreticulin
HMGB1
α-tubulin
B
Relative density
Control
Dox
Vaccine
Dox & Vaccine
eIF2A
Calreticulin
HMGB1
C
Control
Dox
Vaccine
Dox & Vaccine
eIF2A IHC
Calreticulin Immunofluorescence
Mammary tumor
Pulmonary tumor
HMGB1 IHC
D
eIF2A
Ratio of positive cells
Control Dox Vaccine Dox & Vaccine
E
Calreticulin
Relative intensity of mammary tumor
Control Dox Vaccine Dox & Vaccine
F
Calreticulin
Relative intensity of Lung tumor
Control Dox Vaccine Dox & Vaccine
G
HMGB1
Ralative intensity
Control Dox Vaccine Dox & Vaccine

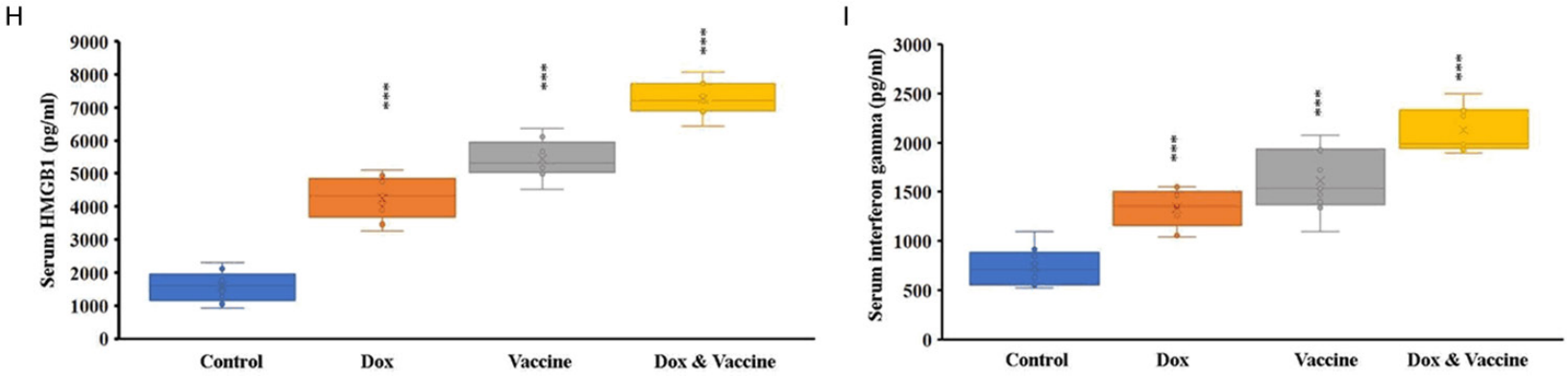

Figure 9. Key elements involved in ICD in mice from different groups. (A, B) Dynamic changes in expression profiling of ER stress marker (eIF2α), "Eat me signal" calreticulin (CALR) and HMGB1 on tumor cells, a ligand of TLR4 on dendritic cells (DCs). (C) Expression and subcellular localization of ICD components in mice from different groups. (D-G) Quantification of (C). (H, I) Release of HMGB1 and IFNγ in mice's serum from different groups. $^{*}P<0.05$; $^{**}P<0.01$; $^{***}P<0.001$; $^{****}P<0.0001$ compared to corresponding control (Student's t-test). Data are presented as mean ± SD calculated from each experiment performed in triplicate under each condition.

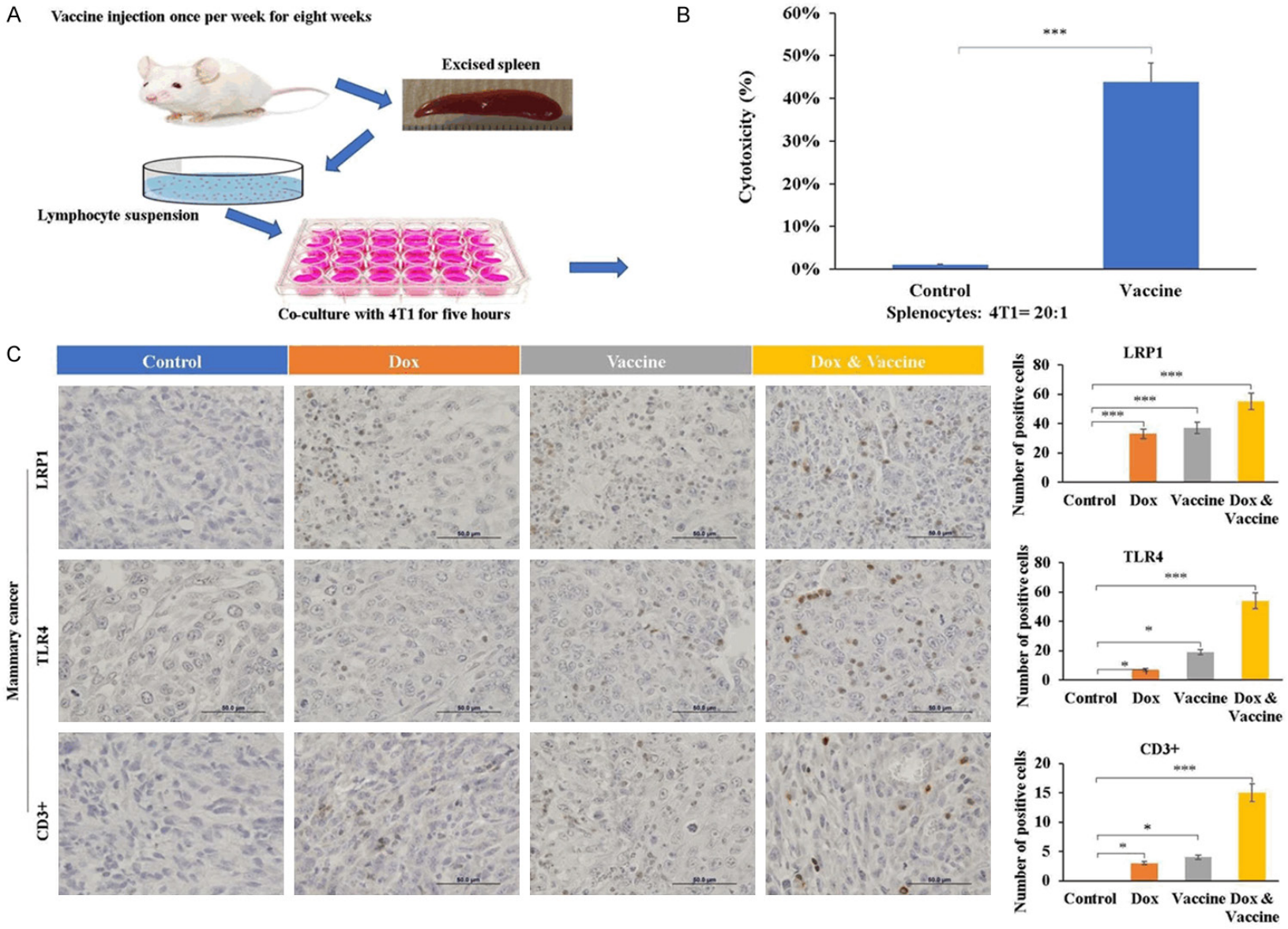
A
Vaccine injection once per week for eight weeks
Excised spleen
Lymphocyte suspension
Co-culture with 4T1 for five hours
B
Cytotoxicity (%)
60%
50%
40%
30%
20%
10%
0%
***
Control
Vaccine
Splenocytes: 4T1= 20:1
C
Control
Dox
Vaccine
Dox & Vaccine
Mammary cancer
LRP1
TLR4
CD3+
LRP1
TLR4
CD3+
Number of positive cells
Control
Dox
Vaccine
Dox & Vaccine

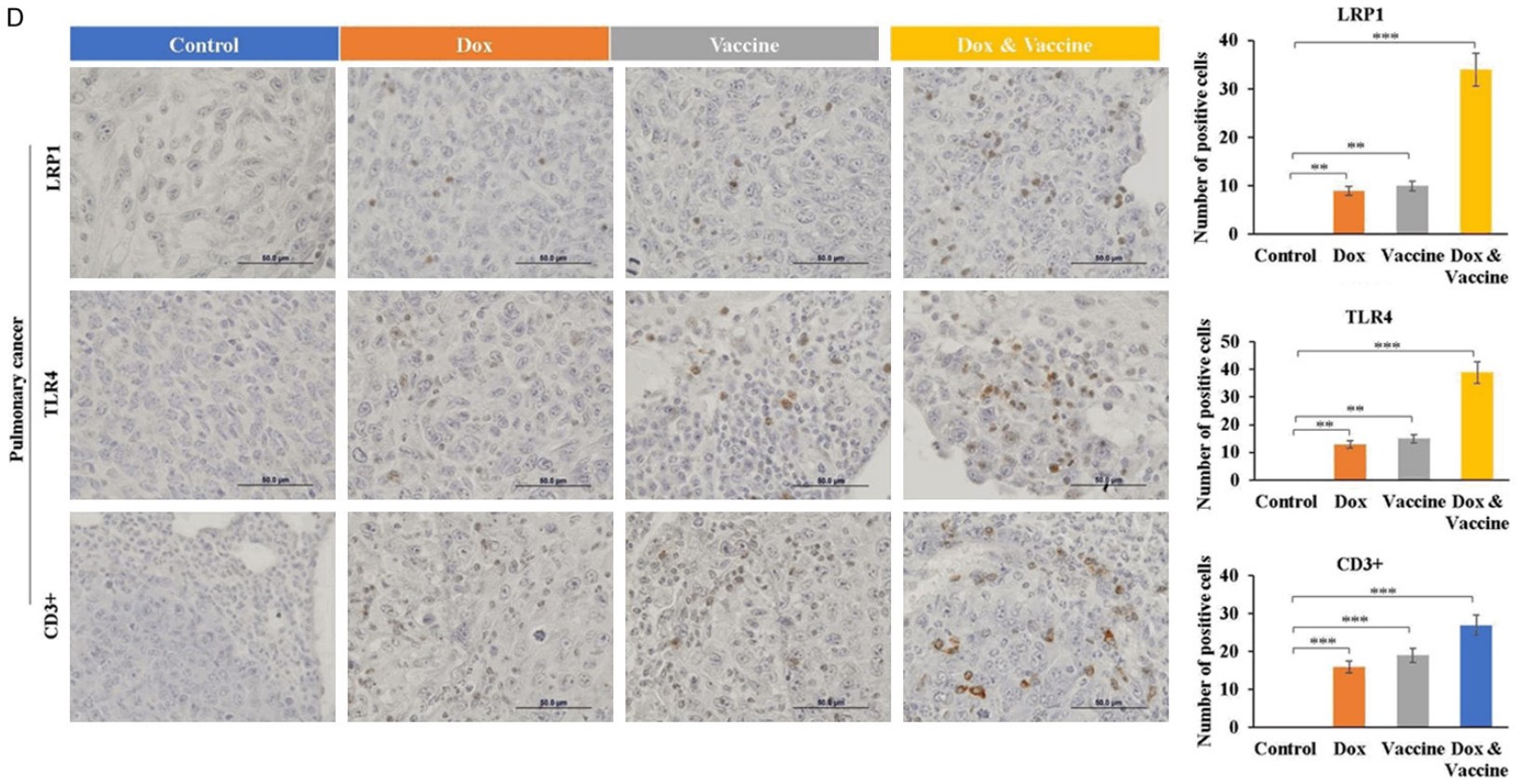

Figure 10. ASPH-based λ phage vaccine enhances antitumor immune response. (A) Scheme of *in vitro* cytotoxicity assay. (B) Compared with control group, cytotoxicity of splenocytes in mice from Vaccine group has been increased by approximate 45 folds. (C, D) Expression profiling of markers for activated and maturated DCs as well as TILs in (C) primary mammary tumors or (D) pulmonary metastatic lesions in mice from different groups. $^{*}P<0.05$; $^{**}P<0.01$; $^{***}P<0.001$; $^{****}P<0.0001$ compared to corresponding control (Student's t-test). Data are presented as mean ± SD calculated from each experiment performed in triplicate under each condition.

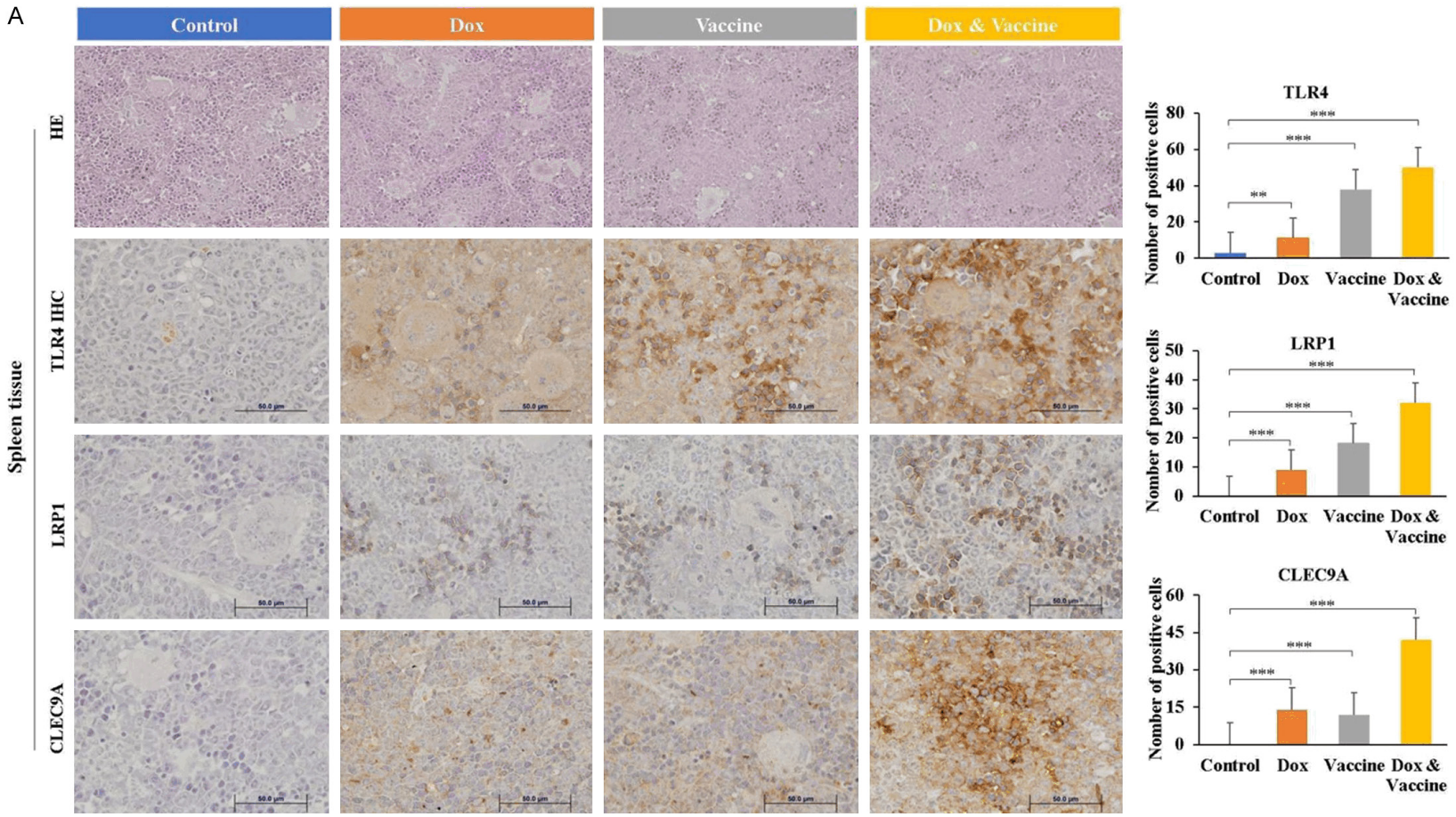
A
Control
Dox
Vaccine
Dox & Vaccine
Spleen tissue
HE
TLR4 IHC
LRP1
CLEC9A
TLR4
Nomber of positive cells
80
60
40
20
0
Control
Dox
Vaccine
Dox & Vaccine
LRP1
Nomber of positive cells
50
40
30
20
10
0
Control
Dox
Vaccine
Dox & Vaccine
CLEC9A
Nomber of positive cells
60
45
30
15
0
Control
Dox
Vaccine
Dox & Vaccine

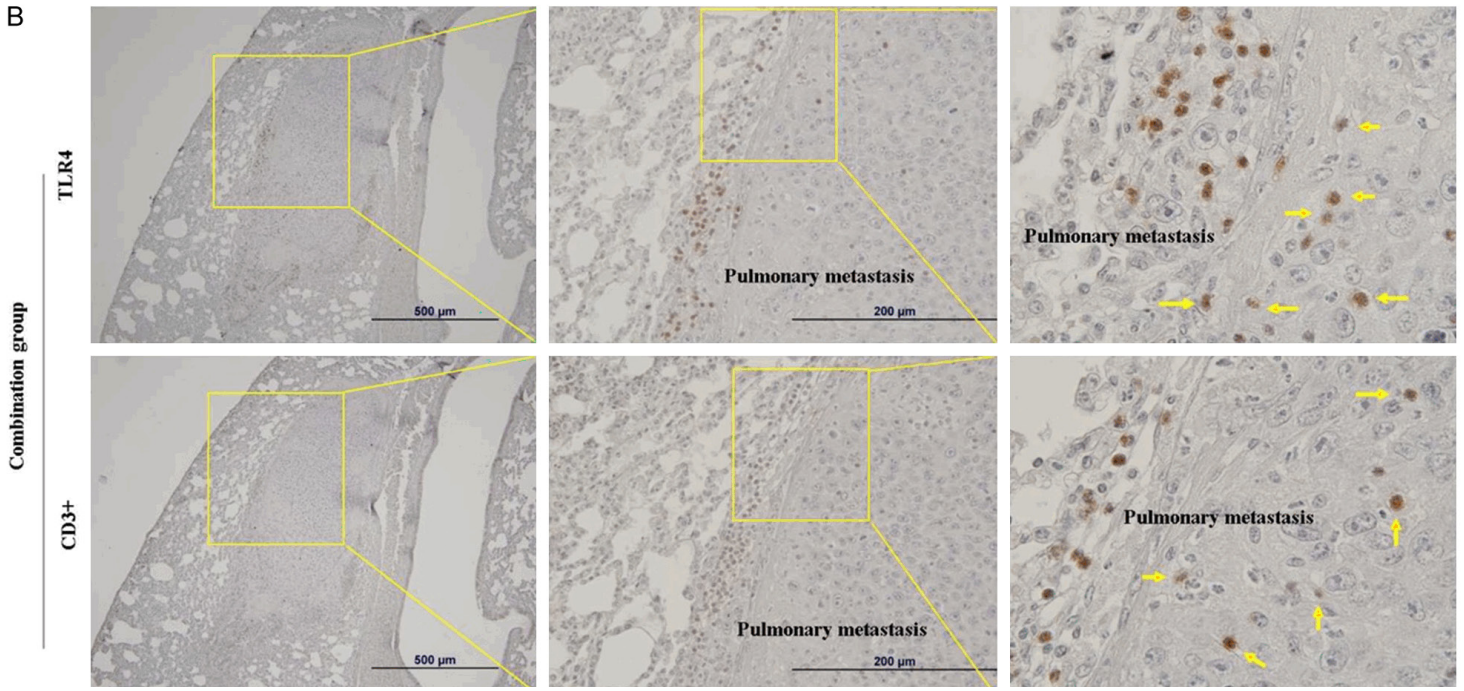
B
Combination group
TLR4
CD3+
500 μm
Pulmonary metastasis
200 μm
Pulmonary metastasis
500 μm
Pulmonary metastasis
200 μm
Pulmonary metastasis

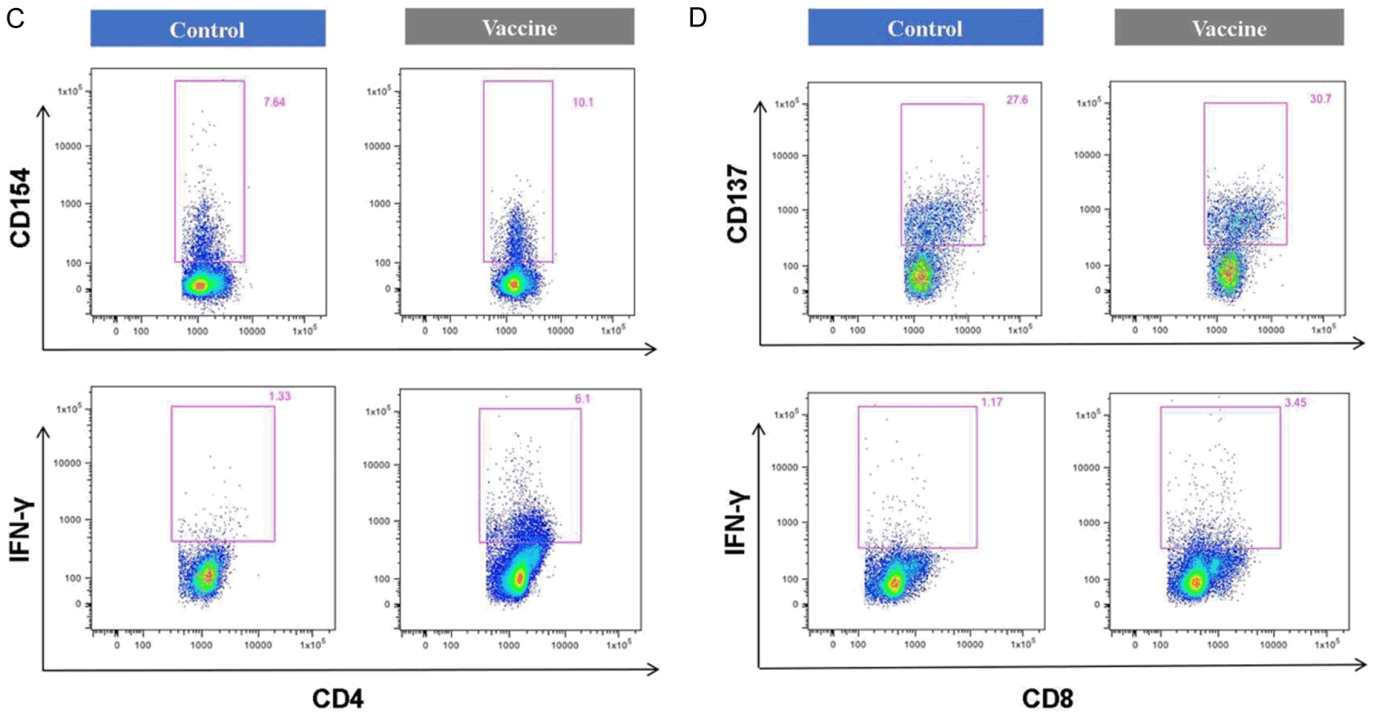

Figure 11. ASPH-based λ phage vaccine stimulates adaptive immune response. A. Expression profiling of DC maturation marker TLR4 in the spleen of mice from different groups. B. Infiltration of maturated DCs and $CD3^+$ T lymphocytes into pulmonary lesions of mice from DOX+Vaccine group. C, D. Compared to control group, combinatory treatment substantially spurs activation of $CD4^+$ and $CD8^+$ cells attributed to antitumor response in mice from DOX+Vaccine group. $^*P<0.05$; $^{**}P<0.01$; $^{***}P<0.001$; $^{****}P<0.0001$ compared to corresponding control (Student's t-test). Data are presented as mean ± SD calculated from each experiment performed in triplicate under each condition.

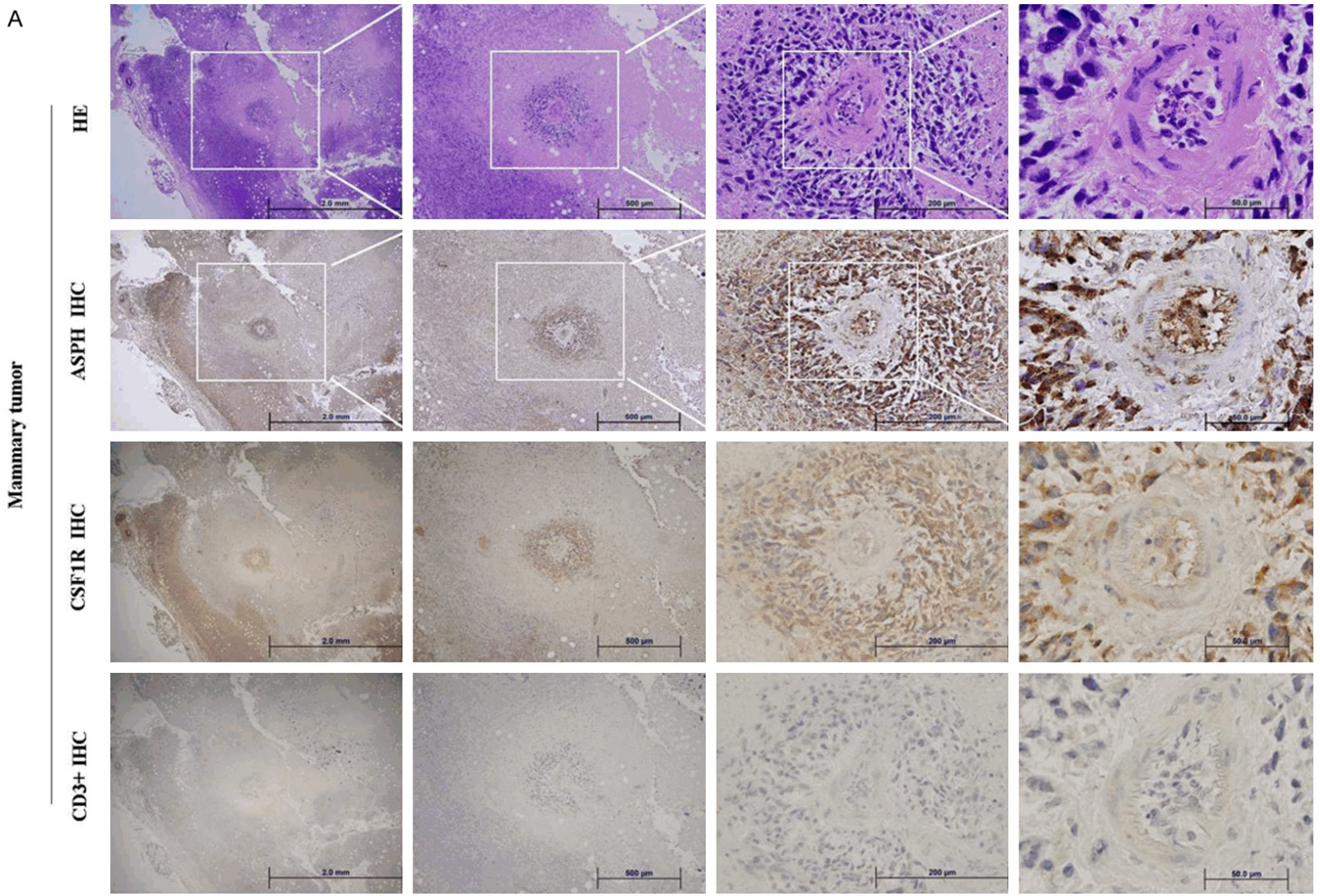
A
Mammary tumor
HE
ASPH IHC
CSF1R IHC
CD3+ IHC
2.0 mm
500 μm
200 μm
50.0 μm

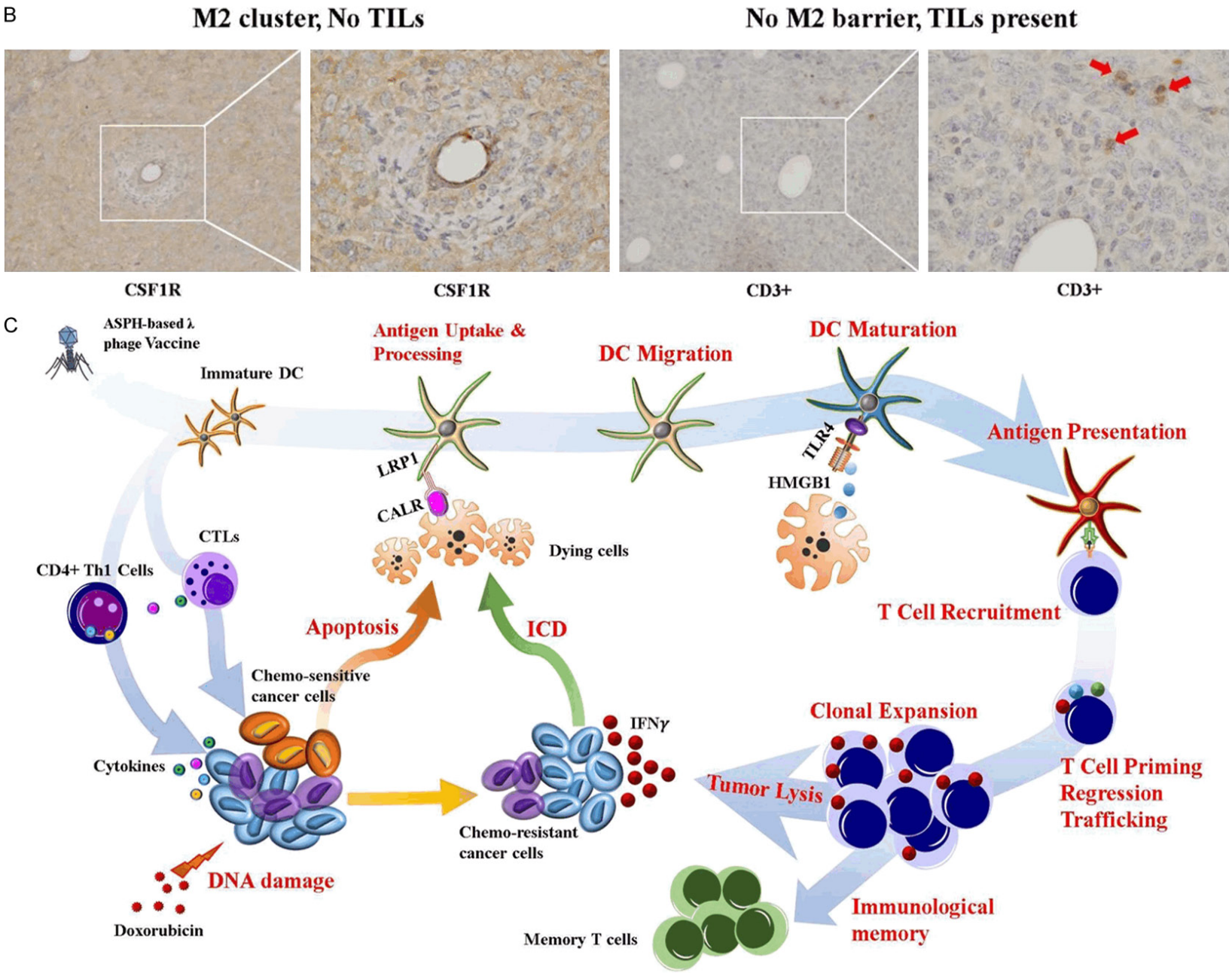
B
M2 cluster, No TILs
No M2 barrier, TILs present
CSF1R
CSF1R
CD3+
CD3+
C
ASPH-based λ phage Vaccine
Immature DC
Antigen Uptake & Processing
DC Migration
DC Maturation
Antigen Presentation
LRP1
CALR
Dying cells
TLR4
HMGB1
CTLs
CD4+ Th1 Cells
Apoptosis
ICD
T Cell Recruitment
Chemo-sensitive cancer cells
IFNγ
Clonal Expansion
Cytokines
Tumor Lysis
T Cell Priming
Regression
Trafficking
Chemo-resistant cancer cells
DNA damage
Doxorubicin
Memory T cells
Immunological memory

Figure 12. Immune suppressive microenvironment edited ASPH expressing breast cancer. A. A classic cancerous nest formed by primary mammary tumor cells highly expressing ASPH and numerous $CSF1R^+$ M2 in control group. No TILs were identified. B. Tumor cells are protected from immune attack by recruiting $CSF1R^+$ M2, which acts as a physical barrier for TILs to blocking their access to vasculature system (blood vessels or lymphatics) adjacent to primary mammary tumor in control group. This is vice versa in combination group. C. Hypothesized mechanisms of combinatory immunotherapy and chemotherapy driven ICD in breast cancer. In response to doxorubicin, an inducer of ICD, cancer cells expose CALR on surface, secrete ATP, and release HMGB1. Upon binding to cognate receptors on the surface of myeloid or lymphoid cells, DAMPs favor the uptake of cell corpses and debris thereof by APCs, including DCs in the context of robust immunostimulatory signals, eventually leading to the priming of an adaptive immune response involving αβ and γδ T cells. This process contributes to the establishment of immunological memory, and thus partially via an IFNγ-dependent mechanism, renders capability to eradicate cancer cells that have survived chemotherapy. APCs, antigen-presenting cells; DAMPs, damage-associated molecular patterns; DC, dendritic cell; ICD, immunogenic cell death; LRP1, LDL receptor related protein 1; TLR4, Toll-like receptor 4.

(error-free repair) to DSBs and SSBs. Mechanistically, ASPH impairs PARP1-/MRN complex-ATM-P53 cascades induced canonical apoptosis. Accumulation of a plethora of errors exacerbates genomic instability. A proportion of dying/dead cancer cells that are sensitive to DOX initiate p-eIF2A-DAMPs (exposure of CALR on surface and passive release of HMGB1) signal to recruit and activate DCs. However, DOX chemo-resistant breast cancer cells with high expression of ASPH will survive and maintain aggressive malignant phenotypes for tumor progression and distant metastasis. A novel λ phage vaccine targeting this tumor associated (TAA), ASPH, on breast cancer cells (sparing normal tissues), impairs this phenomenon. These observations suggest that ASPH-based λ phage vaccine initiates DCs' antigen recognition, uptake and processing, homing to and functional maturation ($CLEC9^+$) at secondary lymphoid organs by enhancing PRRs such as LRP1 and TLR4 expression as well as strengthening LRP1-CALR and HMGB1-TLR4 interactions. This vaccine approach combined with DOX administration successfully induces ICD *in vivo*. Combinatory therapy undermines primary mammary tumor growth and pulmonary metastases generation. Antitumor effects are attributed to clonal expansion of activated helper $CD4^+$ and cytotoxic $CD8^+$ T lymphocytes, which executes tumor lysis (**Figure 12C**).

We have demonstrated that ASPH's oncogenic properties are partially attributed to activation of downstream Notch signaling pathway [16], which regulates cell fate determination and promotes tumorigenesis as emphasized in this study by enhancing cell proliferation and cell-cycle transition. The DNA-damage response (DDR) protects genome stability. Notch1 may suppress DDR by directly binding to ATM regulatory domain FATC to inhibit its kinase activity. The ATM and Notch1 activities were inversely correlated in breast cancer. It is noteworthy that inactivation of ATM by Notch1 enhanced survival of leukemia cells upon DNA damage [18]. Furthermore, Notch1 may inhibit activation of ATM by impairing the formation of ATM-FOXO3a-KAT5/Tip60 complex [19]. These findings, together with the current investigation, emphasize an essential role of ASPH in promoting breast cancer cell survival, as well as resistance to DOX induced DNA damage, to inhibit apoptosis.

The DAMPs are secreted, released or surface exposed by dying/stressed cancer cells, acting as danger signals for the immune system. Specific DAMPs, such as surface-exposed calreticulin, secreted ATP and passively released HMGB1, are preeminent for inducing ICD of tumor cells. Extracellular HMGB1 is pivotal for ICD, but also involved in tumor progression. Multifaceted extracellular HMGB1 may be attributed to different redox states in a context-dependent manner. Here, we have found a contribution of apoptosis-associated HMGB1 release in the context of combination therapy which induces ICD *in vivo* in established breast tumors. The capability of DOX combined with ASPH-based λ phage vaccine to induce ICD may depend, in part, on how well this synergistic effect in parallel or tandemly mediates endoplasmic reticulum (ER) stress and reactive oxygen species (ROS) production. Pre-existing multiple drug-resistant highly expressing ASPH breast cancer cells resist DOX therapy alone. Interestingly, combinatory therapy, an ICD inducer, simultaneously applied with phage vaccine targeting a TAA (ASPH) has reduced this limitation.

Doxorubicin targeting ER, results in ER stress and production of ROS; when combined with ASPH-based λ phage vaccine, subsequently ini-

tiates ICD [6]. In this study, secretion of DAMPs (HMGB1 and CALR) is a hallmark of ICD in breast cancer. Under stress condition (treatment with DOX combined phage vaccine), CALR is translocated from the lumen of ER to the surface of dying cells where it functions as an "eat me" signal for professional antigen-presenting cells [APC]. The CALR exerts immunostimulatory effects by interacting with LRP1 on DCs (or other APC surface receptors) to facilitate uptake, processing, and cross-presentation of a TAA (ASPH) derived from breast cancer cells on MHC class I molecule, initiating $CD8^+$ T cell response. Secreted HMGB1 and ATP are essential DAMPs for ICD amplification [20, 21].

The CALR is expressed in breast cancer cells, and could promote macrophages to engulf hazardous cancer cells. However, most of such cells are not destroyed because of a counterbalance produced by CD47, a special "Don't eat me signal" that blocks CALR [22]. The HMGB1 release to the extracellular space is a prerequisite for an optimal release and presentation of TAAs to DCs. The HMGB1 binds to PRRs expressed on DCs such as TLR2/4. Secreted ATP functions as a "find-me" signal for monocytes and supports their attraction to the site of apoptosis [23].

Interaction between HMGB1 and TLR4 results in upregulation of NF-κB, and thus increased production/release of cytokines. Functionally, HMGB1 regulates changes in DNA architecture essential for repair of DNA damage. In the tumor microenvironment, HMGB1 is secreted by macrophages, monocytes and DCs. Intracellular HMGB1 is a highly conserved chromosomal protein acting as a DNA chaperone. Extracellular HMGB1 is a prototypical DAMP. In this context, HMGB1 may play paradoxical roles in promoting both cancer cell survival and death by regulating multiple signaling pathways, including inflammation, immunity, genome stability, proliferation, metastasis, metabolism, apoptosis, and autophagy [24]. In this study, a high level of ASPH not only inhibits necrosis caused passive release of HMGB1 but also enhances actively secreted HMGB1 to promote tumor progression. However, in response to combinatory treatment, dying/dead cancer cells both passively release and actively secrete HMGB1 to interact with TLR4, resulting in an enhanced DC maturation response.

Bacteriophages are optimal vaccine delivery vehicles attributed to high stability under harsh environmental conditions with potent adjuvant capacities [25]. This ASPH-based λ phage vaccine has efficient immunostimulatory effects. This novel construct expresses multiple copies of ASPH peptides on the surface of immunogenic λ phage particles, thereby eliciting an effective immune response. The ASPH-based λ phage display has shown promise for developing new strategies of vaccine discovery and production. This is a novel approach for a vaccine platform targeting a broad spectrum of ASPH expressing tumors [25].

Conclusion

Collectively, λ phage vaccine targeting a TAA (ASPH) combined with DOX successfully induces ICD and initiates $CD8^+$ T cell-mediated antitumor immunity in breast tumors. The cross-presentation of antigens, especially a TAA (ASPH), derived from dying/dead cancer cells enables DCs to present tumor restricted proteins (in particular ASPH) on MHC class I molecules. This combinatory therapy has exhibited substantial anti-tumor as well as prevents metastatic spread in pre-clinical animal models.

Acknowledgements

We highly appreciate the generosity of Dr. Mark Olsen at the Department of Pharmaceutical Sciences, College of Pharmacy-Glendale, Midwestern University, Glendale (Arizona 85308, USA) for synthesizing, structural characterization and providing data on the purity of small molecule inhibitor of ASPH (MO-I-1182) [13, 16]. This animal study has been approved by the Institutional Animal Care and Use Committee at Rhode Island Hospital/Brown University. This work was supported in part by National Institutes of Health (NIH) (Grant numbers CA123544, P30GM110759) and Institutional Funds of the United States (to J.R.W. and X.Q.D.); National Natural Science Foundation of China (grant number 81670583, to B.S.).

Disclosure of conflict of interest

None.

Abbreviations

ASPH, aspartate beta-hydroxylase; APC, antigen-presenting cell; ATM, ataxia-telangiectasia

mutated kinase; AMPK, 5' adenosine monophosphate-activated protein kinase; BNP-TV, bio-nanoparticle based therapeutic vaccine; CALR, calreticulin; DAMP, Damage-associated molecular patterns; DC, dendritic cell; DOX, Doxorubicin; DSB, double-strand break; eIF2A, eukaryotic translation initiation factor 2A; ELISA, Enzyme-Linked Immunosorbent Assay; HIPK2, homeodomain interacting protein kinase 2; HMGB1, high-mobility group protein 1; ICD, immunogenic cell death; IF, Immunofluorescence; IFNγ, interferon gamma; IHC, immunohistochemistry; KD, knock-down; LRP1, LDL receptor related protein 1; M2, type 2 macrophage; MTT, 3-(4,5-dimethylthiazol-2-yl)-2,5-diphenyltetrazolium bromide; MRN, NSB1/RAD50/MRE11; PARP1, Poly [ADP-ribose] polymerase 1; PCNA, proliferating cell nuclear antigen; PERK, PKR-like ER kinase; PRR, pattern recognition receptor; ROS, reactive oxygen species; SMI, small molecule inhibitor; SSB, single-strand break; TAA, tumor associated; TIL, tumor infiltrated lymphocyte; TLR4, toll like receptor 4; TNBC, triple negative breast cancer; UPR, unfolded protein response.

Address correspondence to: Drs. Jack R Wands and Xiaoqun Dong, Liver Research Center, Rhode Island Hospital, Department of Medicine, The Warren Alpert Medical School of Brown University, 55 Claverick Street, 4th Fl., Providence, RI 02903, USA. Tel: 401-444-2795; Fax: 401-444-2939; E-mail: Jack_Wands_MD@Brown.edu (JRW); Tel: 401-444-5031; Fax: 401-444-2939; E-mail: Xiaoqun_Dong@Brown.edu (XQD); Dr. Bei Sun, Department of Pancreatic and Biliary Surgery, Key Laboratory of Hepatosplenic Surgery, Ministry of Education, The First Affiliated Hospital of Harbin Medical University, No. 23 Youzheng Road, Nangang District, Harbin 150081, Heilongjiang Province, P. R. China. Tel: +86-451-85555721; Fax: +86-451-53643849; E-mail: sunbei70@tom.com

References

[1] Siegel RL, Miller KD and Jemal A. Cancer statistics, 2018. CA Cancer J Clin 2018; 68: 7-30.

[2] Pang B, Qiao X, Janssen L, Velds A, Groothuis T, Kerkhoven R, Nieuwland M, Ovaa H, Rottenberg S, van Tellingen O, Janssen J, Huijgens P, Zwart W and Neefjes J. Drug-induced histone eviction from open chromatin contributes to the chemotherapeutic effects of doxorubicin. Nat Commun 2013; 4: 1908.

[3] Obeid M, Tesniere A, Ghiringhelli F, Fimia GM, Apetoh L, Perfettini JL, Castedo M, Mignot G, Panaretakis T, Casares N, Metivier D, Larochette N, van Endert P, Ciccosanti F, Piacentini M, Zitvogel L and Kroemer G. Calreticulin exposure dictates the immunogenicity of cancer cell death. Nat Med 2007; 13: 54-61.

[4] Kroemer G, Galluzzi L, Kepp O and Zitvogel L. Immunogenic cell death in cancer therapy. Annu Rev Immunol 2013; 31: 51-72.

[5] Galluzzi L, Buque A, Kepp O, Zitvogel L and Kroemer G. Immunogenic cell death in cancer and infectious disease. Nat Rev Immunol 2017; 17: 97-111.

[6] Krysko DV, Garg AD, Kaczmarek A, Krysko O, Agostinis P and Vandenabeele P. Immunogenic cell death and DAMPs in cancer therapy. Nat Rev Cancer 2012; 12: 860-875.

[7] Smith GP. Filamentous fusion phage: novel expression vectors that display cloned antigens on the virion surface. Science 1985; 228: 1315-1317.

[8] Gupta A, Onda M, Pastan I, Adhya S and Chaudhary VK. High-density functional display of proteins on bacteriophage lambda. J Mol Biol 2003; 334: 241-254.

[9] Lin Q, Chen X, Meng F, Ogawa K, Li M, Song R, Zhang S, Zhang Z, Kong X, Xu Q, He F, Bai X, Sun B, Hung MC, Liu L, Wands J and Dong X. ASPH-notch axis guided exosomal delivery of prometastatic secretome renders breast cancer multi-organ metastasis. Mol Cancer 2019; 18: 156.

[10] de la Monte SM, Tamaki S, Cantarini MC, Ince N, Wiedmann M, Carter JJ, Lahousse SA, Califano S, Maeda T, Ueno T, D'Errico A, Trevisani F and Wands JR. Aspartyl-(asparaginyl)-beta-hydroxylase regulates hepatocellular carcinoma invasiveness. J Hepatol 2006; 44: 971-983.

[11] Cantarini MC, de la Monte SM, Pang M, Tong M, D'Errico A, Trevisani F and Wands JR. Aspartyl-asparagyl beta hydroxylase over-expression in human hepatoma is linked to activation of insulin-like growth factor and notch signaling mechanisms. Hepatology 2006; 44: 446-457.

[12] Ogawa K, Lin Q, Li L, Bai X, Chen X, Chen H, Kong R, Wang Y, Zhu H, He F, Xu Q, Liu L, Li M, Zhang S, Nagaoka K, Carlson R, Safran H, Charpentier K, Sun B, Wands J and Dong X. Aspartate beta-hydroxylase promotes pancreatic ductal adenocarcinoma metastasis through activation of SRC signaling pathway. J Hematol Oncol 2019; 12: 144.

[13] Aihara A, Huang CK, Olsen MJ, Lin Q, Chung W, Tang Q, Dong X and Wands JR. A cell-surface beta-hydroxylase is a biomarker and therapeutic target for hepatocellular carcinoma. Hepatology 2014; 60: 1302-1313.

[14] Iwagami Y, Casulli S, Nagaoka K, Kim M, Carlson RI, Ogawa K, Lebowitz MS, Fuller S, Biswas B, Stewart S, Dong X, Ghanbari H and Wands JR. Lambda phage-based vaccine induces an-

titumor immunity in hepatocellular carcinoma. Heliyon 2017; 3: e00407.
[15] Shimoda M, Tomimaru Y, Charpentier KP, Safran H, Carlson RI and Wands J. Tumor progression-related transmembrane protein aspartate-beta-hydroxylase is a target for immunotherapy of hepatocellular carcinoma. J Hepatol 2012; 56: 1129-1135.
[16] Dong X, Lin Q, Aihara A, Li Y, Huang CK, Chung W, Tang Q, Chen X, Carlson R, Nadolny C, Gabriel G, Olsen M and Wands JR. Aspartate beta-Hydroxylase expression promotes a malignant pancreatic cellular phenotype. Oncotarget 2015; 6: 1231-1248.
[17] Sendoel A, Dunn JG, Rodriguez EH, Naik S, Gomez NC, Hurwitz B, Levorse J, Dill BD, Schramek D, Molina H, Weissman JS and Fuchs E. Translation from unconventional 5' start sites drives tumour initiation. Nature 2017; 541: 494-499.
[18] Vermezovic J, Adamowicz M, Santarpia L, Rustighi A, Forcato M, Lucano C, Massimiliano L, Costanzo V, Bicciato S, Del Sal G and d'Adda di Fagagna F. Notch is a direct negative regulator of the DNA-damage response. Nat Struct Mol Biol 2015; 22: 417-424.
[19] Adamowicz M, Vermezovic J and d'Adda di Fagagna F. NOTCH1 inhibits activation of ATM by impairing the formation of an ATM-FOXO3a-KAT5/Tip60 complex. Cell Rep 2016; 16: 2068-2076.
[20] Ghiringhelli F, Apetoh L, Tesniere A, Aymeric L, Ma Y, Ortiz C, Vermaelen K, Panaretakis T, Mignot G, Ullrich E, Perfettini JL, Schlemmer F, Tasdemir E, Uhl M, Genin P, Civas A, Ryffel B, Kanellopoulos J, Tschopp J, Andre F, Lidereau R, McLaughlin NM, Haynes NM, Smyth MJ, Kroemer G and Zitvogel L. Activation of the NLRP3 inflammasome in dendritic cells induces IL-1beta-dependent adaptive immunity against tumors. Nat Med 2009; 15: 1170-1178.
[21] Apetoh L, Ghiringhelli F, Tesniere A, Obeid M, Ortiz C, Criollo A, Mignot G, Maiuri MC, Ullrich E, Saulnier P, Yang H, Amigorena S, Ryffel B, Barrat FJ, Saftig P, Levi F, Lidereau R, Nogues C, Mira JP, Chompret A, Joulin V, Clavel-Chapelon F, Bourhis J, Andre F, Delaloge S, Tursz T, Kroemer G and Zitvogel L. Toll-like receptor 4-dependent contribution of the immune system to anticancer chemotherapy and radiotherapy. Nat Med 2007; 13: 1050-1059.
[22] Chao MP, Jaiswal S, Weissman-Tsukamoto R, Alizadeh AA, Gentles AJ, Volkmer J, Weiskopf K, Willingham SB, Raveh T, Park CY, Majeti R and Weissman IL. Calreticulin is the dominant pro-phagocytic signal on multiple human cancers and is counterbalanced by CD47. Sci Transl Med 2010; 2: 63ra94.
[23] Garg AD, Krysko DV, Verfaillie T, Kaczmarek A, Ferreira GB, Marysael T, Rubio N, Firczuk M, Mathieu C, Roebroek AJ, Annaert W, Golab J, de Witte P, Vandenabeele P and Agostinis P. A novel pathway combining calreticulin exposure and ATP secretion in immunogenic cancer cell death. EMBO J 2012; 31: 1062-1079.
[24] Kang R, Zhang Q, Zeh HJ 3rd, Lotze MT and Tang D. HMGB1 in cancer: good, bad, or both? Clin Cancer Res 2013; 19: 4046-4057.
[25] Aghebati-Maleki L, Bakhshinejad B, Baradaran B, Motallebnezhad M, Aghebati-Maleki A, Nickho H, Yousefi M and Majidi J. Phage display as a promising approach for vaccine development. J Biomed Sci 2016; 23: 66.